CONTRACTOR REPORT

SAND80-8181
UC-62d
Unlimited Release

Corrosion of Alloys in Molten Nitrates

University of Buffalo Foundation, Inc.

Prepared by Sandia National Laboratories, Albuquerque, New Mexico 87185 and Livermore, California 94550 for the United States Department of Energy under Contract DE-AC04-76DP00789.

Printed September 1982

1st Annual Report

May 5, 1980 - June 30, 1981

To: Sandia Laboratories
Livermore, California 94550

Title: Corrosion of Alloys in Molten Nitrates

Contractor: University of Buffalo Foundation, Inc.
250 Winspear Avenue
Buffalo, New York 14215
Attention: E. P. Schneider

Principal Investigator: Dr. Robert A. Osteryoung
Department of Chemistry
State University of New York at Buffalo
Buffalo, New York 14214
Phone: 716-831-3820

Research Associate: Dr. Hector Fernandez

CONTRACTOR'S TECHNICAL REPORT

CONTRACT NO. 20-4478

SANDIA REQUESTOR R. Carling

CONTRACTING REPRESENTATIVE Jack P. Hubner

SANDIA REPORT NO. SAND 80-8181

SF 6432-CTR

CONTENTS

EXECUTIVE SUMMARY

As a portion of a broad based effort involving studies of heat transfer fluids for solar collectors, we initiated work in support of efforts by Sandia National Laboratory and others to utilize molten nitrates as such fluids. Initially, the intent had been to study the behavior of a variety of metal ions at high temperatures in the $(K,Na)NO_3$ binary molten salt. In all this work, a gold electrode of relatively large area was employed as a reference electrode and was checked for stability against a Ag/Ag(I) electrode. We first investigated the behavior of glassy carbon as a potential indicator electrode; it behaved rather similarly to prior investigations of Pt and Au indicator electrodes in these melts in that evidence indicated that NO_3^- reduction, passivation and dissolution processes at the glassy carbon electrodes were about the same as those found for Pt or Au electrodes. On the other hand, the anodic limit of the melt, at the electrode, at relatively low temperatures (<300°C), was shifted to more cathodic values than at either Pt or Au, and, as the temperature was raised, the behavior of the electrode became sufficiently complex that further studies were abandoned.

The behavior of platinum and gold as indicator electrodes was studied up to 550°C. Although both electrodes behave in a similar manner, with increased complexity of the electrode reactions taking place in the pure melt as the temperature is raised, it was determined that Pt appeared to behave in a simpler, more reproducible manner than did gold. Both electrodes showed evidence of attack if prolonged reduction of NO_3^- were performed at the electrode surface.

As a result of DOE funding limitations, it was decided to initiate corrosion studies on Fe, Ni and Incoloy 800 at a much earlier date than

intended, so as to supply as much useful information to Sandia as possible; Incoloy 800 is the material intended for use in the temperature range 550-600°C as container material for the molten nitrates in the solar collector system. Open circuit potentials for Fe, Ni and Incoloy 800 could be obtained, with times varying from a few minutes to several hours. Incoloy 800 open circuit potential was close to, but more noble than that of iron. The presence of chromate in the melt - chromate has been found to be the major soluble corrosion product of Incoloy 800 in a molten nitrate test loop in work performed by Sandia - resulted in open circuit potentials less noble than in its absence.

Current-potential curves at iron, nickel and Incoloy 800 were investigated. Anodic polarization curves on both Fe and Ni exhibited the same general features, an initial jump in potential, followed by a region where the potential changes without appreciable change in current, followed by a region where, it is assumed, nitrite oxidation (only on iron) and Incoloy 800 is observed, followed by a region where the current starts to increase markedly. Potential reversal resulted in, essentially, a retrace of the current-potential curve obtained when scanning the voltage in the anodic direction.

The anodic polarization curves on Incoloy 800 were much different, and much more revealing. The shape resembled that for iron, with an initial potential region to around 0.5 V which is presumed to be a passive region, followed by a NO_2^- oxidation wave, which is followed by a sharp and sudden increase in current, the potential (the breakdown potential) at which this increase in current takes place being less anodic at lower than at higher temperatures. For instance at

250°C, a breakdown potential, where the current increases dramatically, takes place at about 0.9 V; this shifts to about 1.2 V at 450°C. If the scan is reversed once this large increase in current is noted, a very large closed current loop is obtained, i.e., there is significant hysteresis compared to iron or nickel. This closed current loop diminishes markedly as the temperature is raised. Observation of the electrode surface after a series of experiments at various temperatures supports the conclusion that the large current loop is characteristic of an alloy which undergoes crevice and/or pitting corrosion. At 550°C, for instance, a much smaller open current loop is found (less hysteresis), which is suggestive of only pitting corrosion. Observation of the electrode surface after experiments at 550°C showed a brown oxide film, but no evidence of the much greater corrosion found at 250°C. We can thus conclude that the higher the temperature, the stronger and more protective is the initially formed surface oxide film.

INTRODUCTION

This work describes experimental studies performed over the past fourteen months. The initial aim was to study the behavior of metal ions and various metals, from the point of view of their corrosion, in molten nitrates at elevated temperatures, i.e., 500-600°C. The impetus for this work evolved from investigations at Sandia National Laboratories, where research aimed at the possible use of molten nitrates, mainly the equimolar binary mixture of potassium nitrate - sodium nitrate, as thermal heat transfer fluids in solar collectors, is being performed.

Initially, the intent of our work was to begin by studying the behavior of a variety of metal ions at high temperatures in these melts; although a great deal of work has been performed in nitrate melts at lower temperatures (300°C) very little has been done in the elevated temperature range of concern to those interested in using molten nitrates as heat transfer fluids in solar collectors. Although we had performed research in molten nitrates many years ago, our experience was limited to the lower temperatures. To initiate our work, one of the first items was the investigation of an electrode, heretofore unstudied, which we felt might be of use as an indicator electrode for the study of metal solute ions in this melt. Thus, the experimental work on glassy carbon electrodes was initiated. Other indicator electrodes which might prove useful in molten nitrates for the study of solute species at elevated temperatures, platinum and gold, were also investigated; although employed at lower temperatures in nitrate melts, nothing had been done at the temperatures with which we were concerned.

When pronounced changes in funding of DOE projects were indicated to us several months ago, we decided to change direction and to initiate work that it was felt would be much more directly and hopefully immediately applicable to Sandia's interests. Hence the work on the behavior of iron, nickel and Incoloy 800 was initiated, at a much earlier time and at much higher temperatures than we might have wished given optimum conditions for performance of this research. What follows, then is a report on progress from May, 1980 through June 30, 1981.

Part 1. EXPERIMENTAL

Two different experimental cells were employed, one for work with the glassy carbon (GC) electrodes at temperatures up to 350°C, the other for the study of potential indicator electrodes, Pt and Au, and for corrosion studies on Fe, Ni and Incoloy 800.

The first electrochemical cell was made of pyrex glass following conventional design. Its assembly permits the introduction of three electrodes (working, reference and counter), thermocouple probe and gas bubbling inlet and exit. The working electrode consisted of spectroscopic glassy carbon rods of 3 mm diameter sealed under vacuum into pyrex tubes. It was polished with alumina powder on a polishing cloth until a mirror like surface was obtained, and was then washed with distilled water and dried under vacuum. A disc surface of 0.07 cm^2 resulted. The counter electrode was a platinum spiral placed in a separate fritted compartment. The reference electrode was a Ag/Ag^+ ($AgNO_3$ 0.08 m) electrode isolated by means of fritted compartment from the cell proper. $NaNO_3$ (Baker) and KNO_3 (Fisher) were recrystallized, oven dried under vacuum and further dehydrated by bubbling dry nitrogen or oxygen slowly through the melt.

The experiments were carried out in the temperature range 224-351 $\pm$1°C under Ar.

The electrochemical container cell for the high temperature work was made of quartz. The cell head has five joints to accommodate the electrodes, gas inlet and thermocouple compartment and a gas outlet. Teflon sleeves were used to assure a good seal. A pure gold crucible was employed to contain the melt. A schematic of the cell is shown in

Figure 1. A variety of metal wires were used as working electrodes. Pt, 0.05 cm, and Au, 0.05 cm, were supplied by Engelhardt and were 99.9%. Fe, 0.0125 or 0.25 cm, and Ni, 0.05 cm, were supplied by Alpha Products and were 99.99% pure. Numbers refer to wire diameter. In some experiments Alfa Products 99.99% Fe foil was used. Either square or cylindrical cross section rods of Incoloy 800 alloy obtained from Sandia were used.

All of the metal surfaces were polished with emery paper and finally polished with 0.3 μm alumina powder on a polishing cloth with water. The counter electrode was a spiral platinum wire in either a quartz tubing (small holes in the bottom of the tube assured electrical contact with the melt) or a Pyrex tube with a fritted disc to avoid diffusion of species from this compartment to the melt. The reference electrode was either platinum or gold wire dipped directly into the melt or the gold crucible, or in some cases a gold foil in a Pyrex tube containing the same melt, electrical contact being established through a fritted disc.

Experience has shown that reasonably large area noble metal electrodes, such as Pt or Au, perform reasonably satisfactorily in molten salts as reference electrodes. While not poised, they attain and maintain stable potentials. Care must be exercised in that the introduction of a redox reagent, such as dichromate, will shift the potential of such a quasi-reference. Under such circumstances the electrode must be separated from the indicator electrode compartment, as described below.

After several experiments, the platinum wire became brown; because of this, gold wire or (in most of the experiments) the gold crucible

was preferred for use as a reference electrode. Gold surfaces do not appear to suffer any change in the melt unless subjected to prolonged electrolysis (see below) and it has been shown that they have a stable reference potential. In some experiments, for reasons mentioned above, the reference gold foil was separated from the bulk melt by a fritted disc. All potentials are reported against the potential of the gold crucible. A chromel-alumel thermocouple, connected to a temperature controller, served as a temperature probe, and was inserted into a quartz tube dipped into the melt. A gold-deposited quartz furnace was used. The quartz or pyrex tube compartments, for the counter electrode, the thermocouple and the gold foil reference electrode were covered with gold foil to minimize the glass contact with the melt. The initial geometrical area of the working electrode samples was used to calculate the current densities.

The concentration of nitrite ion after the melt is equilibrated with oxygen is around 0.34 M (mean value of several determinations with samples taken during different days). The concentration of nitrite ion was determined by potentiometric titration using excess $KMnO_4$ standard solution and then back titration with Fe(II) standard solution. This is in agreement with previous work.[1]

Part 2. STUDIES OF GLASSY CARBON, PLATINUM AND GOLD AS INDICATOR ELECTRODES

2.1 Glassy Carbon (G.C.) Electrodes

No references on the use of glassy-carbon (G.C.) electrodes in $(K,Na)NO_3$ melts have been reported in the literature. Graphite has been studied by Arvia et al.[2-3] in this melt, and due to the fact that G.C. is gaining popularity as a solid inert electrode for electrochemical studies, some attempt was made to elucidate its behavior in molten alkali nitrates, as well as to compare its electrochemical properties with those of platinum, gold and graphite.

2.1.1. Preliminary Results

When a G.C. electrode is dipped into a "pure" nitrate melt at 254°C, an initial potential of around -0.30 V is observed but after about 30 minutes a value of -0.23 V was attained. This tendency was observed at all working temperatures but at higher temperatures, the time to reach stable potentials decreases. In melts containing added nitrite the rest potential is more cathodic than in the pure melt but changes to more anodic values when the temperature increases. Equilibrium potentials attained were reasonably reproducible after the fresh electrodes had been cycled at least three times between -0.20 and +0.60 V.

2.1.2. Cathodic Runs

Results similar to those obtained at Pt electrodes[4] and graphite electrodes[3] in the nitrate melt systems were found with the G.C. electrode. The following observations were made on voltammograms running from -0.2 to -2.0 V.

a) The cathodic current peak which is related to the electrochemical reduction of $NO_3^- \rightarrow NO_2^-$ and the simultaneous formation and precipitation

of an alkali metal oxide on the electrode. The maximum current shifts towards more cathodic potentials when the potential scan rate was increased from 50 to 300 mv/sec (Fig. 2). A linear dependence was found between peak potential and the square root of the sweep rate (Fig. 3) and between peak current and square root of sweep rate (Fig. 4), which is typical of the variation expected for a precipitation-dissolution process under ohmic control.[5]

b) An anodic current peak at around -1.1 V was assigned to the electrochemical dissolution of the oxide which also shifts with the rate of potential scan. Peak currents increased linearly as the square root of the scan rate, with a slope of approximately 0.3 mA $mV^{-1/2}$ $s^{1/2}$ and the anodic peak potential was linear in the log of the scan rate with a slope of approximately 80 mV per decade change in scan rate, over scan rates of 50 to 300 mV s^{-1}.

c) An anodic current peak located at around -0.35 V which probably corresponds to the discharge of the O_2^- ion.[4] This peak is seen only when the melt is electrolysed at potentials more cathodic than at -1.5 V. With both platinum[4] and graphite,[3] the current peak at -0.35 V appears well defined during the first potential scan. However, on G.C. electrodes no cathodic current peak is observed in the same potential region (Fig. 5). This perhaps indicates a difference in the catalytic ability of the G.C. electrode compared to graphite or Pt. When oxygen was bubbled through the melt for several hours, neither a change in the shape of the peaks referred to above nor new peaks were observed. This indicates that there is little specific reaction of the melt with oxygen and probably also indicates that the solubility of oxygen in the melt is quite low.

d) As the temperature increases, the cathodic current peak increases and the peak potential shifts to more anodic values. A plot of cathodic peak potential against temperature is linear with a slope of 1.85×10^{-3} V/°C over the temperature range 250-350°C. This variation is similar to that obtained at Pt electrodes in these nitrate melts, indicating a similar mechanism.[5] The anodic peak potential located at -1.1 V at 254°C also shifts but to more cathodic values and the current peak decreases as the temperature increases. As determined from the voltammograms, the ratio between the anodic charge and the cathodic charge (Q_a/Q_c) decreases with an increase in temperature. The anodic peak located at -0.35 V (at 254°C) is no longer obtained at higher temperature. If O_2^- is the ion that is discharged at this potential at lower temperatures, the absence of this peak at higher temperatures could result from the equilibrium $\frac{1}{2} O_2 + O^{=} \rightleftarrows O_2^{2-} \rightleftarrows O_2^- + e^-$ shifting to the left as the temperature increases.

2.1.3. Anodic Oxidation of Nitrite

The oxidation wave located at around +0.5 V is due to the discharge of NO_2^- ion.[6,7] A melt 8.45×10^{-3} M in nitrite was prepared to check the behavior of this ion under anodic polarization at several temperatures. Fig. 6 shows cyclic voltammograms carried out between -0.2 and +0.65 V at 224°C (a) and 254°C (b). As can be noted, the best defined anodic wave corresponds to that obtained at the lowest temperature; after reversing the potential, a wide cathodic wave is obtained. At 351°C, the anodic and cathodic waves do not appear at all, probably due to the fact that they are masked by electrochemical reactions of nitrate ions, whose overvoltage decreases appreciably as the temperature is increased.[3]

As shown in Fig. 7, if the cathodic run is allowed to go to more cathodic potentials than -0.2 V, a well defined peak can be obtained at around -0.25 V, indicating creation of a product that can be reduced.

2.1.4. Anodic Runs and Pre-anodization in Pure Melt

Anodic runs were performed starting from -0.2 V, reversing (switching) the potential sweep at +0.6 or +0.7 V and recording the cathodic voltammogram to -1.2 V. In some experiments a waiting time of 25 sec was employed at the switching potential.

The shape of the cathodic voltammogram depends on both the reversing potential and waiting time at the reversing potential; in every case, the oxidation wave of residual nitrite is obtained during the initial anodic run. When the potential sweep is reversed at +0.6 V a wide reduction wave can be observed at around +0.2 V as shown in Fig. 8, and no other wave or peak appears until -1.2 V. If the anodic potential sweep is stopped at +0.6 V for 25 sec. and then the cathodic scan recorded, the peak at +0.2 V is now wider and a new cathodic peak is obtained at around -0.25 V (similar to that shown in Fig. 7, in the melt with added nitrite). A small shoulder is also observed at around -0.45 V. Similar effects can be noted if the scan reversal occurs at +0.7 V; the cathodic peak at -0.25 V is smaller than that in the previous experiment and slightly shifted to anodic potentials (Fig. 9a). When the anodic potential sweep is stopped at +0.7 V for 25 sec. and then a cathodic scan recorded, the peak located at +0.2 V disappears and a new large peak is obtained at around -0.55 V. If a new voltammogram is run between -0.2 and +0.6 V after the prior experiment, without polishing the electrode, it shows larger anodic currents and a total absence of

cathodic peaks in this range of potential, indicating the presence of film or electrode reaction product on the surface.

When the current sensitivity is increased five times a small, new anodic peak was obtained at +0.25 whose height increased linearly with the square root of the sweep rate. (This small anodic peak was also found by Arvia et al. in the melt employing graphite electrodes.[3]) After reversing the potential at +0.3 V (before the discharge of NO_2^- takes place) a wide cathodic peak is observed at +0.1 V. After reversing the potential at more anodic values, the cathodic peak at +0.2 V is obtained again.

2.1.5. Summary

Since this study of G.C. electrodes was initiated to determine if these electrodes could be employed as indicator electrodes in the study of soluble species in these melts, and since the problems described above clearly increased with increasing temperature, this work was terminated.

However, from the results shown above, there is evidence indicating that NO_2^- reduction, passivation and dissolution processes at G.C. electrodes are about the same as at platinum electrodes, but G.C. apparently does not show catalytic properties for the discharge of ionic species of oxygen (or even traces of water) which are remarkably enhanced at platinum surfaces. On the other hand, the anodic limit of this melt at a G.C. electrode is shifted to more cathodic values than at platinum or even at graphite, almost overlapping the anodic oxidation wave of nitrite. Other complications also appear on the anodic side.

2.2 Platinum Electrodes

The study of the cathodic as well as the anodic behavior of this

metal at different temperatures was intended to establish the potential range for the performance of electrochemical studies of soluble species as products of Incoloy 800 corrosion in this melt.

2.2.1. Cyclic Voltammograms at Different Temperatures

Cathodic cyclic voltammograms starting from zero volts for platinum at temperatures ranging from 285-550°C are shown in Fig. 10. Their characteristics are similar to those reported previously,[5] for temperatures up to 400°C. Two cathodic peaks appear at around -1.55 V and -1.78 V respectively and they shift to more anodic values as the temperature increases. The first peak is due to the nitrate reduction-passivation process from the formation of an insoluble film (assumed to be sodium oxide).[4,8] The second cathodic peak is much smaller than the first and its nature is still obscure, despite several investigators having cited it.[8,9] The higher the temperature, the higher the peak current of both of these waves and the closer their peak potentials. Above 500°C the second peak loses definition and, as can be seen from Fig. 10d and 10g, very high cathodic currents are obtained after the first cathodic peak. The activation energy is 11 Kcal/mol, in agreement with that reported by other authors.[8,9] The variation of the peak potential vs temperature is linear up to 450°C and agrees quite well with that reported by Arvia,[5] and that obtained with a G.C. electrode (see above).

After reversing the potential at -1.8 V, a cathodic bump can be observed at around -1.5 V and its position is apparently independent of the temperature. Above 348°C it is no longer observable (Fig. 10c).

This peak is connected to the second cathodic peak mentioned above, because if the scan is reversed before the cathodic peak, the bump does not appear during the anodic scan.

After reversing the potential scan at -1.8 V, a large anodic peak is obtained at around -0.95 V which corresponds to the anodic dissolution of the passivating film formed during the first cathodic run. Its peak potential shifts to more cathodic values as the temperature increases (up to around 450°C) and its peak current decreases with temperature. Above 500°C it is no longer observable. It is probable that this phenomenon is associated with an increase of solubility of the passivating film with temperature; this is supported by the fact that above 500°C a large cathodic current due to the continuing reduction of nitrate is obtained up to around -1.15 V during the anodic scan which then drops rapidly to low cathodic values without passing to the anodic side of the voltammogram.

A small wave is also seen during the anodic scan at -0.5 V which is attributed to the oxidation of superoxide ion present in the melt and the product of the anodic dissolution of the passivating film according to Zambonin,[4] but it loses definition above 400°C. At the highest temperature (550°C) the surface of the platinum electrode shows attack after each experiment if the voltage scan is carried to very cathodic potentials.

Thus, the cathodic limit of the melt is shifted to more anodic potentials as the temperature increases. The suitable limit for the study of soluble species in this melt at 550°C is about -0.55 V, after which the reduction of NO_3^- takes place.

Anodic voltammograms are shown in Fig. 11 for the 250-550°C temperature range. The reversible peaks for the NO_2^-/NO_2 couple are clearly seen (note arrow in Fig. 11a) in Figs. 11a-11c (252-348°C) but for temperatures above 350°C the anodic oxidation peak of NO_2^- overlaps with the NO_3^- oxidation and is no longer observable (Fig. 11e-11g), the overvoltage for the oxidation of NO_3^- to NO_2 and O_2 being lowered as the temperature increases.[3] The potential for the NO_2/NO_2^- peaks are in agreement with those previously reported.[7] The higher the temperature the higher the anodic currents. It is not possible to determine the activation energy for NO_2^- oxidation because its concentration changes with temperature.[10-13] At 550°C the anodic limit of the melt is around +0.5 V.

2.3 Gold Electrodes

As for platinum, this study was intended to determine the suitability of gold as an indicator electrode for the study of soluble species in these nitrate melts at elevated temperatures.

2.3.1. Cyclic Voltammograms at Different Temperatures

Cathodic voltammograms for a gold electrode are shown in Fig. 12. The characteristics of the first catahodic peak (located at around -1.5 V at 258°C, Fig. 12a) are quite similar to those obtained for Pt electrodes. However, its activation energy is lower, approximately 9 kcal/mol. The second cathodic peak does not appear at the lower temperatures in the range of potentials studied, but does start to appear at 348°C (Fig. 12c) shifting to more anodic potentials with temperature. Apparently, it overlaps with the first cathodic peak (Fig. 12d). As with Pt, the presence of this after-peak causes the appearance of another cathodic peak during the anodic scan after potential reversal

(Figs. 12c-d). Very high cathodic currents are obtained at the highest temperatures after reversing the potential scan as shown in Figs. 12d-12g. The surface of the gold electrode shows signs of attack after this experiment at the high temperature presumably the result of interaction of a product generated at the high cathodic currents with the electrode surface. The most significant difference between the cathodic runs for Au and Pt is that for Pt electrodes no cathodic peak appears before the reduction peak of NO_3^- for all temperatures, but for Au electrodes a shoulder appears at around -0.92 V at 398°C (Fig. 12d), is converted to a wave at -0.85 V (448°C, Fig. 12e) and to a definite peak at -0.7 V at temperatures above 500°C (Figs. 12f, 12g,h, 12i,j). Since this peak does not appear when Pt is used instead of Au, we feel that this peak is a characteristic of gold rather than the melt itself. Thus, the cathodic limit of the melt is 100-150 mV less cathodic at Au than at platinum.

After reversing the potential scan, the anodic runs show more complicated current-potential curves at Au than at Pt. For the lowest temperature the anodic peak for the oxidation of the passivating film generated during the cahtodic scan is broader and its peak current decreases more rapidly with the temperature than in the case of Pt. Its peak potential shifts to more cathodic values for the lowest temperatures (Fig. 12a-b). For temperatures above 300°C it is not possible to establish a systematic behavior for this peak. At intermediate temperatures, a wave (peak) appears at around -0.9 V (Figs. 12b-e) but again no correlation can be established.

At 550°C a well defined anodic peak can be observed at -0.68 V (Fig. 12g) which is connected with polarization at more cathodic potentials,

because if the cathodic scan is reversed after the cathodic peak at -0.7 V, no anodic peak is obtained at that potential (Fig. 12h-i). Also, depending on the switching potential, two very close anodic peaks which overlap each other can be obtained between -0.5 V and -0.2 V (Fig. 12j)

The anodic peak for the oxidation of O_2^- to O_2 (according to Zambonin),[4] is well defined at the lowest temperature (Fig. 12a). It appears at around -0.5 V and it becomes broader and shifts to more anodic values when temperature increases (Fig. 12a-d). So, comparing the i-E cathodic curves for Au and Pt, it seems that despite the complexity of both systems, Pt electrodes behave in a simpler and more reliable manner than Au for performing electrochemical studies of soluble species in this melt. It has to be pointed out that visible attack is seen at both metals only when the potential scan is carried to very cathodic potentials in the region of NO_3^- reduction; on the other hand, repetitive cycling between 0 V and -0.5 V did not show any visible surface attack on Pt.

Anodic cyclic voltammograms for gold are shown in Fig. 13. They show the same characteristics as those previously described for anodic voltammograms obtained using platinum electrodes. However, it must be pointed out that if a second anodic run is performed without removing the gold electrode for polishing (for instance at 250°C where the peaks of NO_2^- /NO_2 couple are best defined) a different voltammogram is obtained, showing a shift of the peak potential of the oxidation of NO_2^- to more anodic values and loss of peak definition. We can thus conclude that the gold surface changes in some way during the anodic sweep. With Pt electrodes repetitive sweeps give quite reproducible anodic voltammograms even at the highest temperatures.

2.4 Summary

The study of the glassy carbon, platinum and gold electrodes was initiated to determine if these electrodes could be employed as indicator electrodes in the study of soluble species in these melts.

The results on glassy carbon indicated that NO_3^- reduction, passivation and dissolution processes at these electrodes were similar to those at Pt or Au. G.C., however, appears not to show the catalytic properties for the discharge of ionic species of oxygen (or even traces of water) which are enhanced at platinum surfaces. The anodic limit of the melt at a G.C. electrode is shifted to more cathodic values than at platinum or gold, or even at graphite, almost overlapping the anodic oxidation wave of nitrite. Other complications also appear on the anodic side. Since these problems clearly increase with increasing temperature, the work with G.C. electrodes was terminated at temperatures of approximately 350°C, and no further work was performed.

Platinum and gold showed somewhat similar behavior, and both could be utilized to 550°C. Two cathodic peaks appear at both electrodes; the first involves nitrate reduction, and the precipitation of Na_2O at the surface, forming a passivating film, as observed at lower temperatures. The origin of the second wave is unknown. In general, one large anodic wave, corresponding to the removal of the passivating film, is found; this anodic behavior is more complex on Au than on Pt. Some evidence for a surface reaction involving the Au electrode is presented. Both electrodes appear to show the waves for superoxide oxidation. Both electrodes also indicate the presence of the NO_2^-/NO_2 couple. Pt shows some evidence of surface attack after electrochemical cycling at the

highest temperatures employed. Because of the apparent surface reaction involving gold, we conclude that at least at the highest temperature (550°C), Pt is somewhat better as an indicator electrode than Au.

Part 3. CORROSION BEHAVIOR OF Fe, Ni AND INCOLOY 800

3.1 Introduction

The study of the anodic behavior of Fe[14-16] and Ni[8,16-18] in KNO_3-$NaNO_3$ melts has been carried out in recent years, but usually at temperatures not exceeding 350°C. Measurements of corrosion rates for Fe in $NaNO_3$ and KNO_3 have been determined using gravimetric methods at temperatures up to 470°C by Notoya et al.[19] and for mild steel in the $(Na,K)NO_3$ eutectic by A. Baraka et al,[20-22] who also reported anodic polarization of mild steel in the absence[23] as well as in the presence of acidic and basic species.[24] Gurovich[25] obtained corrosion data for Ni, carbon steel and other metals by studying the weight change after short immersion of the samples in $(Na,K)NO_3$ melts at 400-500°C. Reactions of several metals, including iron, chromium and nickel, in molten $(Li,K)NO_3$ were studied to establish the main reaction products yielded by decomposition of the melt.[26] All the data reported in the literature indicate that iron and nickel passivate spontaneously in contact with $(K,Na)NO_3$ melt[14,17,19,23] giving no detectable amount of ionic species of these metals in the fused salts. The passivating films are mainly Fe_3O_4 and NiO respectively, as determined by X-ray difractometry. These findings agree with thermodynamic considerations.[27-30]

Chromium metal does not appear to have been studied in this melt,[31] since it reacts with $(Li,K)NO_3$ melt to yield $CR_2O_7^{=}$ which is soluble.[26] Above 350°C, $Cr_2O_7^{=}$ also reacts with the melt yielding $CrO_4^{=}$.[32]

Incoloy 800 alloy (I800) (45.1% Fe, 31.2% Ni, 21.2% Cr, 0.92% Cu and other minor constituents) has received much attention the past few years ago because it has a stable, fully austenitic structure and high strength combined with resistance to oxidation, carburization and

corrosion in a wide variety of aggressive industrial environments at elevated temperatures.[33] Several corrosion studies have been performed in different media at high temperature, such as water, steam, helium, liquid metls, molten halides, etc.,[33,34] with the purpose of determining if its use is feasible in high temperature steam generation systems. The only reference found in the literature by the authors regarding electrochemical studies of I800 is related to potentiodynamic polarization experiments in NaOH solutions at 250°C.[33] In most of the cases, depletion of chromium from the alloy is associated with corrosion behavior.[33] With regard to I800 corrosion behavior in $(K,Na)NO_3$ melt there is no work in the literature, except for recent reports of investigators at Sandia National Labs,[1,35] who are investigating I800 as container material to be employed in a solar collector using $(K,Na)NO_3$ as the collector fluid. R. W. Bradshaw has found that the metal surface is covered by an outer film of Fe_3O_4 and an intermediate mixed oxide spinel $(Fe,Cr)_3O_4$ whose thickness ratio depends upon temperature.[35] Chromium depletion from the alloy into the $(K,Na)NO_3$ melt as soluble $CrO_4^{=}$ is the other main feature, apparently according to diffusion-limited kinetics.[35] Above 600°C the corrosion rate of the alloy, as shown by Bradshaw, is drastically increased.

The purpose of work in this section is to provide electrochemical data on the behavior of Fe, Ni, and I800 in $(K,Na)NO_3$ melt to supplement corrosion data obtained by Bradshaw et al.

3.2 Open Circuit Potential (OCP)-Time Curves for Iron, Nickel and Incoloy 800:

The potential of iron, nickel and I800 electrodes under open circuit conditions in $(K,Na)NO_3$ melts were followed as a function of time

until steady-state values were established. The curves in Fig. 14-17 show the OCP behavior at different temperatures. For some of the curves in that figure, the final potentials in the figure do not necessarily represent the steady-state values which are sometimes reached after a longer period of time, but the aim in presenting such a time scale is to show more clearly the variations of OCP at relatively short times. A steady state value is considered to have been achieved when the OCP was constant to ± 5 mV for one hour. In any case, the OCP shifts in a more noble direction immediately after immersion for all temperatures examined, indicating that the electrodes became passivated when in contact with the melt.

3.2.1. Iron

Steady-state potentials were obtained after periods ranging from 1-2 hours depending on the working temperature; the higher the temperature the shorter the time taken to reach steady values (Fig. 14). The OCP-t variation and the temperature coefficient of steady-state potentials ($\sim$ 1mV/°C) for iron are in agreement with those reported by Baraka et al[20] for mild steel. The passivating film is mainly formed by an iron oxide of the structure of magnetite (Fe_3O_4).[14,19,20,22] At 550°C, a stable steady-state potential of -0.015 V is reached after about 1 hour immersion.

3.2.2. Nickel

With Ni electrodes the OCP reaches a steady-state potential in a much shorter time than in the case of iron, as can be seen in Fig. 15. A feature different from that of iron is that the short time potential variation is not totally reproducible but a drop of OCP to more noble

potentials after a short time of immersion is still found at the intermediate temperature studied. After a maximum value, the OCP then decreases until it reaches its steady-state value. The origin of this phenomenon is obscure. The passivating film is thought to be mainly NiO.[16-18] It is not possible to establish a definite relationship between steady-state potential and temperature. At 550°C, a stable steady-state potential of +0.002 V is attained after about 6 minutes of immersion.

3.2.3. Incoloy 800 Alloy

Variations of OCP of I800 with time are shown in Figs. 16-17. The overall trend is intermediate between that of iron and nickel. The steady-state potential values tend to be closer to those of iron at the same temperature, but more noble and are attained in a slightly shorter period of time. After immersion of I800 electrode in the melt, OCP vs t shows a sharper drop of potential to more noble values than in the case of iron, and after the OCP passes a maximum it shifts to more cathodic potentials until it attains its steady-state value. The variation is similar but smoother than that obtained with nickel electrodes. In Fig. 17 OCP vs t curves are shown for I800 in melts containing different concentrations of potassium chromate at 547°C. It is observed that the initial as well as the steady-state potentials tend to be less noble for higher $CrO_4^{=}$ concentration. The variation of the OCP is also smoother for higher $CrO_4^{=}$ concentrations than in the absence of this species. OCP vs t is also shown in Fig. 17 for an I800 electrode which was previously dipped in the melt until it attained its steady-state potential, removed, washed thoroughly with distilled water, dried and again immersed in the melt. It is interesting to note that the initial potential is almost

the same as the steady-state potential reached before it was removed from the melt and washed. Then the OCP drops slightly to more noble values and then nearly returns to the former value. This experiment clearly suggests that the passivating film is strongly attached to the electrode surface and does not change its properties after removal and washing. The dependence of the steady-state potential on temperature is linear up to 450°C with a temperature coefficient of 1 mV/°C, similar to iron. For the highest temperatures reached the temperature coefficient is less than 1 mV/°C. At 550°C, a stable steady-state potential of -0.005 V is attained after about 40-50 minutes.

3.3 Current - Potential Curves for Iron, Nickel and I800:

A systematic study was performed for these metals covering a wide range of temperature. After preliminary tests using different polarization techniques, the automatic potential-scan technique was chosen because it gave the most reproducible data in our hands as well as others.[36,37] A potential scan rate of 0.2 mV/sec was used, unless otherwise specified. All the anodic polarization experiments were started only after the electrodes reached their steady-state potentials.

3.3.1. Iron

Potential-log current density plots are shown in Fig. 18 covering the range of temperature between 258-548°C. The curves are characterized by an initial increase of anodic current at potentials near the OCP; the current then continues to increase much more slowly with the subsequent increase in potential. At more anodic potentials (around +0.5 V for the lowest temperature) nitrite-iron oxidation takes place and a net limiting current is established. On further increase in potential,

there is a sudden increase in current. The morphology of the E/log i curves have the same shape at all temperatures investigated. The higher the temperature the higher the currents on the first part of the E/log i curve as well as the limiting oxidation current of NO_2^-. The oxidation wave of NO_2^- also shifts to more anodic potentials when the temperature is increased. Typical active-passive transitions were not found. An explanation of these phenomena may be postulated as follows. It is well known that pure iron[14] as well as steel[15,19,20] react spontaneously with fused nitrates to produce magnetite as a surface passivating oxide. The corrosion potential of iron (and even nickel) is more anodic than that corresponding for the metal/metallic ion and metal/metal oxide couples, but more cathodic than other possible redox reaction.[28] For $(K,Na)NO_3$ the possible redox reactions may be:

$$2\ NO_3^- + 1e \rightleftarrows 2\ NO_2^- + O_2^- \qquad (1)$$

$$NO_3^- + 2e \rightleftarrows NO_2^- + O^{2-} \qquad (2)$$

$$2\ NO_3^- + 2e \rightleftarrows 2\ NO_2^- + O_2^{2-} \qquad (3)$$

or, in the presence of NO_2^- ion, the reduction process may be[28]

$$NO_2^- + e \rightleftarrows NO + O^{2-} \qquad (4)$$

In this case, any reaction involving O_2^- or O_2^{2-} can be considered negligible, because NO_2^- tends to stablilize the O^{2-} ion.[4,28] It is reasonable to assume that both reactions 2 and 4 participate in the passivation of iron, taking into account with Notoya[19] has observed regarding the small amount of gaseous products evolved from the specimen at the initial stage of oxidation, but with NO_2^- being the main product; (the same results have been found in this laboratory). In any case, the reduction reaction is a highly effective cathodic process which leads

iron to a spontaneous stable passive state.[38] This explanation is supported by the fact that if the E/log i curves are recorded from positive to negative potential, the initial curve is reasonably well reproduced and the potential reaches a rather stable value quite close to the initial steady-state potential while the current becomes very low and constant (dotted lines of Fig. 19). After such experiments pure iron electrodes show a block brittle surface film. Thus, at the time the polarization experiment starts, the electrode surface is already passivated by the passivating oxide film. Precathodization apparently does not affect the E/log i curves, at least at the sweep rate used in these experiments. Passive currents as well as limiting currents for NO oxidation are shown in Table 1. The experimental activation energy determined by plotting log i_p vs 1/T is E_a = 26 Kcal/mol (Baraka[20] determined a value of Ea = 17.0 Kcal/mol for mild steel in the same melt under air atmosphere, while the values determined by Notoya[19] were 33.8 and 35.0 Kcal/mol in $NaNO_3$ and KNO_3 respectively). In Fig. 20 cyclic voltammograms for iron at 547°C are shown. Cathodic runs started at different immersion times indicate the reduction of the surface oxide. For comparison purposes, the current-potential curve (i-E) for platinum is also shown.

3.3.2. Nickel

E-log i curves for nickel electrodes are shown in Fig. 21 at different temperatures. They exhibit the same features over the entire range of temperatures investigated. Thus, a small increase of the electrode potential from its steady-state value causes the current to increase rapidly, but, as with iron, further increase in potential causes a much smaller increase in current (passive current), as seen in

the potential region up to around +0.6 V for the lowest temperature experiments and up around +0.9 for the highest temperature experiments. At potentials more anodic than those values the current starts to increase more rapidly and massive dissolution of the electrode has been noted as soluble Ni^{+2} in the melt at current densities above 15 mA/cm.[3,17] No limiting current for the oxidation NO_2^- is obtained. A similar result was found by Arvia et al in the same system but a lower temperatures.[17] If the potential is reversed before the dissolution potential, the E/log i curve obtained (dotted lines on Fig. 21) reproduces the former quite well. The rest potential is again very near the initial steady-state value. Anodic linear sweep potential scans gave erratic traces in agreement with the results of Swofford.[8] The color of the electrode surface depends upon the electrolysis conditions. At potentials up to +0.4-+0.5 V the electrode exhibits a straw-colored surface. At potentials below the dissolution potential the surface is bright and after the dissolution potential, the electrode shows a black film (presumably NiO) and diminution of area. It has been previously determined that nickel (as iron) is spontaneously passivated when in contact with alkali nitrate melts,[16-18] NiO being the passivating oxide. No active-passive transition was found, perhaps for the same reason as that of iron above. Passive currents are shown in Table 1. The experimental activation energy calculated from the slope of log i_p vs 1/T plot is E_a = 25 Kcal/mol.

3.3.3. Incoloy 800

E/log i plots for I800 at different temperatures are shown in Fig. 22. Their shapes resemble those obtained for iron, i.e. an initial potential region to around 0.5 V where the passive current increases relatively slowly after a sudden increase near the steady-state potential

and then a limiting current for the oxidation of NO_2^- (which is not so well defined as in the case of iron), but the anodic limit is attained at less anodic potentials. A few millivolts after the NO_2^- wave, the current increases very rapidly, this effect being much more pronounced at the lower temperatures studied. For instance, if an anodic polarization run is performed at 250°C at a sweep rate of 0.1 mv/sec to very anodic potentials and then the potential scan is reversed, the E/log i curve obtained is showed in Fig. 23a. A tremendous increase in current is observed at around +0.9 V (breakdown potential) immediately after the NO_2^- oxidation wave. At +0.91 V the potential scan is reversed (now ν = 5 mv/sec) and a big closed current loop is obtained. At a potential of -0.015 V the E/log i curve on the reverse scan crosses that of the forward scan. If a second experiment is performed with a clean electrode (Fig. 23b), the E/log i characteristic shows somewhat different features. The steady-state potential shifts to more anodic values, the passive currents are higher than in the previous experiment and their potential region is largely diminished. Also, the NO_2^- oxidation wave shifts to more cathodic potentials and the breakdown potential is now around +0.5 V. A large closed current loop is again obtained and the E/log i curve crossing appears at the same potential as in the previous experiment. In both cases, the rest potential tends very slowly to the initial steady-state value. The E/log i curve obtained in the second experiment shows clearly that melt properties have changed in some way as a consequence of products formed at the electrode surface or in the melt during the first experiment. After these experiments the melt shows an orange color and a brown/red precipitate. If cyclic voltammograms are now recorded using platinum as a working electrode, no peaks are seen during

the first anodic run, but a cathodic peak is located at around -0.52 V during the cathodic run (Fig. 24a). After reversing the potential at -0.6 V only one anodic peak at around +0.03 V is obtained. If the potential is held at -0.6 V for 20 seconds and then the anodic run performed, the anodic peak at +0.03 V is shifted slightly to a more anodic value and its peak current increases. A second small anodic peak is now observed at around +0.45 V. The cathodic peak at -0.52 V is attributed to the reduction of $Cr_2O_7^{=}$ ion giving as products Cr_2O_3 and $CrO_4^{=}$, as found by Derivaz.[39] Cr_2O_3 is a solid film whose anodic oxidation gives rise to the anodic stripping peak located at +0.03 V. The small anodic peak found at +0.45 V is assumed to result from the oxidation of $CrO_4^{=}$ to $Cr_2O_7^{=}$ and O_2. These findings are supported by the voltammograms obtained after small additions of $K_2Cr_2O_7$ (Fig. 24b) and K_2CrO_4 (Fig. 24c) to the melt. Thus, it is reasonable to assume that the main product of the corrosion of the electrode at high anode potentials at 250°C is soluble $Cr_2O_7^{=}$ and some solid iron oxide (Fe_2O_3).[14] Some of the results of Derivaz[39] were not confirmed here, but it must be pointed out that the concentration range of $Cr_2O_7^{=}$ and $CrO_4^{=}$ in these experiments differ remarkably from that used by the cited author. The presence of the corrosion products in the melt changes the potential of the gold crucible reference electrode, which is unpoised, as verified by checking against a Ag/Ag^+ (0.08 m) reference electrode. To avoid this difficulty, an isolated gold foil electrode (described in the experimental part) was used as a reference. Its stability was checked against the same Ag/Ag^+ reference electrode.

The surface of the I800 electrode after the experiment of Fig. 23a shows very defined grain boundaries as well as pits spread out over the

surface. Apparently, the immersed surface closer to the melt/oxygen interface is more strongly attacked. The surface of the sample from the experiment in Fig. 23b shows much more attack than the previous sample due to the fact that the sweep rate following scan reversal of the E/log i curve was much slower in this case (0.1 mv/sec). If the potential scan is reversed before the sudden current increase, no closed loop is observed, i.e., there is much more of a retrace character to the curve as in Fig. 19 for Fe, and the final rest potential is practically the same as the initial steady-state potential. The electrode surface is now covered by a thin transparent light blue film. At all the temperatures studied, a brown gas was evolved from the electrode when high currents were passed. The sudden increase of current after a certain potential (breakdown potential) and the closed current loop observed in Fig. 23 are characteristics of an alloy which suffers localllized corrosion (crevice and/or pitting corrosion) in an aggressive media.[37] The breakdown potential is usually called the "critical pitting potential (E_B)" and the potential where both forward and reverse scans intersect is called the "protection potential (E_p)". They are labeled in Fig. 23. Alkali nitrate melts are rich in aggressive species, such as NO_3^-, NO_2^- (which is a product of the decomposition of the melt[10,11,40] as well as of the reaction between the electrode and the melt),[19] OH^- (which is a product of the reaction of residual water with ions such as $O^=$, O_2^{2-} or O_2^- present in the melt)[4] and NO_2 under anodic conditions.[17] Observation of the electrode surface after these experiments supports conclusively the phenomenon suggested by the E/log i curves. The concentration of $Cr_2O_7^=$ ions determined after the experiment of Fig. 23b

was about 10^{-4} M, as determined by potentiometric titration using Fe(II).

No active-passive transition was found in any case at all the temperatures studied, the reason perhaps being that given for the iron electrodes. As previously pointed out, the appearance of a closed current loop is greatly diminished when the temperature increases, as seen in Figs. 25-26. At 398°C (Fig. 25) a closed loop, characteristic of crevice corrosion is still observed but is smaller than in the experiments at 250°C. The rest potential attained is more anodic than that at the lower temperatures but again it slowly shifts in the cathodic direction. A close comparison cannot be made because the sweep rate was higher than in the previous experiment. In Fig. 26 both forward and reverse scans at 547°C can be observed. The kind of closed loop now obtained suggests only susceptibility to pitting corrosion.[37] The rest potential, as can be seen in this figure, tends to the steady-state value. After this experiment a very thick brown oxide film was found but no pitting. We conclude that the higher the temperature the stronger and more protective is the surface film against localized corrosion. Cavities and pits have been found in I800 when this alloy is used as tubing for a sodium-cooled fast reactor steam generator, although no satisfactory explanation has been given as to how the cavities form.[33] Passive currents as well as limiting currents for NO_2^- oxidation at I800 are shown in Table 1. The experimental activation energy determined from the slope of log i_p *vs* 1/T plot is E_a = 21 Kcal/mol. It is interesting to note from Table 1 and Figs. 18 (for Fe), 21 (for Ni) and 22 (for I800), that passive currents for I800 are smaller than for iron or

nickel at the same potential, but the I800 breakdown potential is intermediate between iron and nickel for all the temperatures studied.

Attempts were made to establish the anodic behavior of I800 in $(K,Na)NO_3$ melts containing added $CrO_4^{=}$ ions. E/log i curves for different concentrations of K_2CrO_4 at 547°C are shown in Fig. 27. The morphology of these curves is similar to that obtained in melts without $CrO_4^{=}$, but some differences can be observed. The higher the chromate concentration, the higher the passivity current at different potentials (Table 2) and the smaller the nitrite oxidation current. Also, the higher the chromate concentration the more anodic the potential limit of the melt, and the lower the susceptibility to pitting corrosion (Fig. 27d). The narrow range of chromate concentration studied does not permit a definite conclusion about its influence on the I800 behavior. A systematic study covering a wider range of temperature and chromate concentrations should be carried out.

3.4 Summary

Stable open circuit potentials for Fe, Ni and Incoloy 800 could be obtained; the time to achieve the open circuit potential varied from a few minutes to several hours. The OCP of Incoloy 800 were close to, but more noble than, that of Fe. Chromate appears to render the OCP of Incoloy 800 slightly less noble than in its absence.

Current-potential curves for Fe, Ni and Incoloy 800 were generated under a variety of conditions. For Fe and Ni, the anodic polarization curves were rather similar, exhibiting an initial jump in potential, which was then followed by a polarized (passive) region where the potential shifted without appreciable change in current. This is followed, on Fe but not on Ni, by a region where nitrate oxidation is observed; following this, a marked depolarization of the electrode is observed, apparently the result of massive surface oxidation. Potential scan reversal on Fe and Ni results in, essentially, a retrace of the current-potential curve obtained when scanning in the anodic direction.

The behavior of Incoloy 800 was much different. The initial behavior of Incoloy 800 is much like Fe, an initial passive region at around -0.5 V (depending on temperature), followed by the NO_2^- oxidation plateau. Following this, a sharp, drastic increase in current takes place. The potential at which this increase takes place is less anodic at lower temperatures. Scan reversal yields a very large closed current loop, the extent of the loop being much greater at lower than at higher temperatures. These loops are characteristic of crevice and/or pitting corrosion. This is borne out by observation of the electrode surface after a series of experiments at various temperatures. At 250°C, marked

evidence of pitting and crevice corrosion is seen, in accord with the markedly large closed current (hysteresis) loop found at that temperature; at 550°C, it appears that a much more coherent oxide film is formed, which limits the extent of corrosion.

Part 4. QUALITATIVE TESTS

Some qualitative tests were made. Either metallic chromium or chromium trioxide (CrO_3) added to the melt at a temperature around 300°C slowly react evolving brown gas (NO_2) and giving an orange color to the melt. The reactions are highly accelerated as the temperature is raised. $Cr_2O_7^{=}$ solutions also gave the same color, so it is reasonable to assume that the main product of the reactions mentioned above is $Cr_2O_7^{=}$. Previously, Brough et al[26] have found that metallic chromium also reacts in $(Li,K)NO_3$ melt at 300°C giving $Cr_2O_7^{=}$ as a final product. At 550°C, melts containing $Cr_2O_7^{=}$ (orange color) are transformed to yellow colored melts in a few (3-4) hours. The product is assumed to be $CrO_4^{=}$. Brown gas also is evolved (NO_2). This reaction has not been studied in $(K,Na)NO_3$ melt, but Brough et al[32] concluded that $Cr_2O_7^{=}$ reacts with NO_3^- in a $(Li,K)NO_3$ melt giving $CrO_4^{=}$, NO_2 and O_2 above 350-400°C. $Fe(NO_3)_3$ added to the melt at 350°C immediately reacts giving as products a red-brown solid precipitate and brown gas (NO_2). The liquid phase is then completely colorless. No ferric ions were detected by the usual test with SCN^-.

Part 5. REFERENCES

1. "Corrosion Studies in Convection Loops". R. Bradshaw. Molten Nitrates Salt Technology Workshop, Dublin, California, 1980.

2. A. J. Arvia and W. E. Triaca, Anales Asos. Quim. Argentina, 56 (1968) 33.

3. M. G. Sustersic, W. E. Triaca and A. J. Arvia, Electrochim Acta, 19 (1974) 1.

4. P. G. Zambonin, J. Electroanal. Chem., 24 (1970) 365.

5. M. G. Sustersic, W. E. Triaca and A. J. Arvia, Anales Asos. Quim. Argentina, 66 (1978) 229.

6. H. S. Swofford and P. G. McCormick, Anal. Chem., 37 (1965) 970.

7. L. E. Topol, R. A. Osteryoung and J. H. Christie, J. Phys. Chem., 70 (1966) 2857.

8. H. S. Swofford and H. A. Laitinen, J. Electrochem. Soc., 110 (1963) 814.

9. G. J. Hills and K. E. Johnson, Proceeding of the 2nd International Congress on Polarography, Cambridge (1959), p. 974, Pergamon Press, London (1961).

10. E. S. Freeman, J. Phys. Chem., 60 (1956) 1487.

11. E. S. Freeman, J. Am. Chem. Soc., 79 (1957) 838.

12. P. G. Zambonin and J. Jordan, J. Am. Chem. Soc., 89 (1967) 6365.

13. P. G. Zambonin and J. Jordan, J. Am. Chem. Soc., 91 (1969) 2225.

14. A. J. Arvia, J. J. Podesta and R. C. V. Piatti, Electrochim. Acta, 17 (1972) 33.

15. F. F. Faizullin and V. K. Saifullin, Issled. po elektrokhimii, magnetokhimmi i elektrokhim. metodam analiza, 4, Ch. 1 (1974) 28.

16. A. Conte and S. Casadio, Ric. Sci., 36 (1966) 433.

17. A. J. Arvia, R. C. V. Piatti and J. J. Podesta, Electrochim. Acta, 17 (1972) 901.

18. R. Piontelli, U. Bertocci and G. Sternheim, Z. Elektrochem., 62 (1958) 772.

19. T. Notoya and R. Midorikawa, Denki Kagaku, 39 (1971) 930.

20. A. Baraka, A. I. Abdel-Rohman and A. A. El Hosary, Br. Corros. J., 11 (1976) 44.

21. A. A. El Hosary, A. Baraka and A. I. Abdel-Rohman, Br. Corros. J., 11 (1976) 163.

22. A. A. El Hosary, A. Baraka and A. I. Abdel-Rohman, Br. Corros. J., 11 (1976) 228.

23. A. Baraka, A. I. Abdel-Rohman and A. A. El Hosary, Br. Corros. J., 11 (1976) 161.

24. A. Baraka and M. F. El-Ghandour, Br. Corros. J., 11 (1976) 225.

25. E. I. Gurovich, Zh. Prikl. Khim., 29 (1958) 722.

26. B. J. Brough and D. H. Kerridge, Inorg. Chem., 4 (1965) 1353.

27. S. L. Marchiano and A. J. Arvia, Electrochim. Acta., 17 (1972) 25.

28. S. L. Marchiano and A. J. Arvia, Anales Asos. Quim. Argentina, 63 (1975) 17.

29. A. Conte and S. Casadio, Ric. Sci., 36 (1966) 488.

30. S. L. Marchiano and A. J. Arvia, Electrochim. Acta., 17 (1972) 861.

31. "Encyclopedia of Electrochemistry of the Elements". Vol. 10, J. Plambeck, Ed. A. J. Bard, M. Decker, Inc. New York and Basel, 1976.

32. B. J. Brough, D. H. Kerridge and S. A. Tariz, Inor. Chim. Acta., 1 (1967) 267.

33. "A Status Review of Alloy 800". Proceeding of a British Nuclear Energy Society, Ed. S. F. Pugh, AERE Harwell, Oxfordshire, 1975.

34. J. W. Koger, Handbook of Stainless Steel, Eds. D. Pickner and I. M. Bernstein, McGraw-Hill, 1977.

35. R. W. Carling, C. M. Kramer, R. W. Bradshaw, D. A. Nissen, S. H. Goods, R. W. Mar, J. W. Munford, M. M. Karnowsky, R. N. Biefeld and N. J. Norem, "Molten Nitrate Salt Technology-Development Status Report", SAND80-8052, March 1981.

36. N. D. Greene and R. B. Leonard, Electrochim. Acta., 9 (1964) 45.

37. "Electrochemical Techniques for Corrosion". NACE, Houston, Texas, 1976.

38. "Passivity and Protection of Metals Against Corrosion". N. D. Tomashov and G. P. Chernova, Plenum Press, New York, 1967.

39. J. P. Derivaz and J. Augustynski, J. Electroanal. Chem., 61 (1975) 175.

40. R. F. Bartholomew, J. Phys. Chem., 70 (1966) 3442.

Table 1.-Parameters derived from E/log i curves.Pure melt.

T(°C)	E(V)	log i_p($\mu A/cm^2$)	log i_{L,NO_2^-}($\mu A/cm^2$)
Incoloy 800			
250	-0.20	-0.35	1.07
357	+0.10	0.80	2.70
453	+0.20	1.75	3.35
547	+0.20	2.50	4.52
Iron			
250	-0.10	-0.25	1.27
345	+0.20	1.30	3.09
398	+0.30	1.94	3.91
548	+0,20	3.52	5.08
Nickel			
345	+0.15	1.00	
398	+0.20	1.87	
548	+0.30	3.45	

Table 2.-Parameters derived from E/log i curves.Melt with $CrO_4^=$

T(°C)	E(V)	log i_p(A/cm^2)	$C_{K_2CrO_4}$(M)	
547	+0.20	2.50	0	
"	"	2.70	0.001	
"	"	2.80	0.006	Incoloy 800
"	"	2.92	0,010	

FIGURE CAPTIONS

Fig. 1 Electrochemical cell assembly: (a) Quartz vessel, (b) Gold crucible/"quasi" reference electrode, (c) Incoloy 800 alloy working electrode, (d) Counter electrode, (e) Thermocouple, (f) Gas inlet, (g) Gas outlet, (h) Gold sleeves, (i) Gold wire, (j) Silver wire, (k) 55/50 ground quartz joint, (1) "Mini" Ace-thread adapter, (m) Gold-gold seal, (n) Silver-Incoloy 800 junction, (o) hole to prevent pressure differential.

Fig. 2 Voltammograms obtained with the G.C./molten $(Na,K)NO_3$ system starting from -0.20V at different sweep rates (ν): (a) 50, (b) 100, (c) 200, (d) 300 mv/sec, T = 254°C.

Fig. 3 Plot of the peak potential corresponding to the cathodic peak located at -1.8 to -1.9 V vs the square root of the sweep rate G.C./molten nitrate system, T = 254°C.

Fig. 4 Plot of the cathodic current peak at $\sim$ -1.8 V vs the square root of the sweep rate G.C./molten nitrate system, T = 254°C.

Fig. 5 Voltammogram recorded under the same experimental conditions as in Fig. 2b. At A the sensitivity of the recorder was changed.

Fig. 6 Voltammograms for G.C./molten nitrate system starting from -0.20 V at different temperatures with added $NaNO_2$: (a) 224°C, (b) 254°C, $C_{NO_2^-} = 8.45 \times 10^{-3}$ M, ν = 100 mv/sec.

Fig. 7 Voltammogram recorded under the same experimental conditions of Fig. 6b, but showing the reverse cathodic scan to -1.25 V.

Fig. 8 Voltammograms for G.C./molten nitrate system starting from -0.20 V. Potential scan stopped at +0.60 V for: (a) 0 sec, (b) 25 sec, ν = 50 mv/sec, T = 254°C.

Fig. 9 Voltammograms recorded under the same experimental conditions as Fig. 8, but the potential scan stopped at +0.70 V.

Fig. 10 Voltammograms obtained with the Pt/molten nitrate system starting from 0.00 V at different temperatures: (a) 258°C, (b) 300°C, (c) 348°C, (d) 398°C, (e) 448°C, (f) 504°C, (g) 550°C, ν = 100 mv/sec.

Fig. 11 Voltammograms recorded under the same experimental conditions as Fig. 10, but in the anodic direction.

Fig. 12 Voltammograms obtained with the Au/molten nitrate system starting from 0.00 V at different temperatures: (a) 258°C, (b) 300°C, (c) 348°C, (d) 398°C, (e) 448°C, (f) 504°C, (g,h) 550°C, (i,j) 548°C, (a-h), ν = 100 mv/sec; (i,j) ν = 150 mv/sec.

Fig. 13 Voltammograms recorded under the same experimental conditions as Fig. 12a-g, but in the anodic direction.

Fig. 14 Open circuit potential-time curves for iron in molten nitrate system at different temperatures: (○) 257°C, (△) 345°C, (□) 398°C, (◇) 547°C.

Fig. 15 Open circuit potential-time curves for nickel in molten nitrate system at different temperatures: (○) 345°C, (△) 398°C, (□) 548°C.

Fig. 16 Open circuit potential-time curves for Incoloy 800 alloy in molten nitrate system at different temperatures: (○) 250°C, (△) 357°C, (□) 452°C, (◇) 500°C, (▽) 548°C.

Fig. 17 Open circuit potential-time curves for Incoloy 800 alloy in molten nitrate system at different added K_2CrO_4 concentrations: (▽) 0, (○) 0.001, (△) 0.006, (□) 0.010 M. Curve with the symbol (◇) represent the E-t variation of an already passivated electrode, T = 548°C.

Fig. 18 E-log i anodic polarization curves for iron in molten nitrate system at different temperatures: (○) 258°C, (△) 345°C, (□) 398°C, (◇) 548°C, ν = 0.2 mv/sec. On each curve, horizontal arrow indicates the rest potential (OCP) attained after the experiment was completed.

Fig. 19 E-log i anodic polarization curves for iron in molten nitrate system at (○) 250°C and (◇) 548°C, showing the reverse scan, ν = 0.2 mv/sec.

Fig. 20 Voltammograms recorded on the iron/molten nitrate system: (a) Run started after 33 minutes of immersion, (b) after 96 hours of immersion. Dotted line corresponds to the background current for platinum, T = 548°C, ν = 50 mv/sec, A = 0.020 cm^2.

Fig. 21 E-log i anodic polarization curves for nickel in molten nitrate system at different temperatures: (○) 345°C, (△) 398°C, (□) 548°C, ν = 0.2 mv/sec. Dotted lines represent the reverse scan and horizontal arrows rest potentials.

Fig. 22 E-log i anodic polarization curves for Incoloy 800 alloy in molten nitrate system at different temperatures: (○) 250°C, (△) 357°C, (□) 453°C, (◇) 547°C, ν = 0.2 mv/sec. On each curve, horizontal arrow indicates the rest potential attained after the experiment was completed.

Fig. 23 Cyclic E-log i polarization curves for Incoloy 800 alloy in molten nitrate system. Consecutive experiments in the same melt. Sweep rate (ν): (a)— 0.1 mv/sec, ---5 mv/sec/ (b) —— 0.1 mv/sec, ---0.1 mv/sec, T = 250°C, E_B: critical pitting potential; E_p: protection potential.

Fig. 24 Voltammograms recorded using a platinum electrode (A = 0.15 cm^2) in molten nitrate system: (a) 10^{-4} M $K_2Cr_2O_7$. Potential scan stopped at -0.6 V for the specific lapse of times: (I) 0, (II) 20 sec, (b) same as curve (aI) plus a small addition of $K_2Cr_2O_7$, (c) same as curve (b) plus a small addition of K_2CrO_4, T = 250°C, ν = 100 mv/sec.

Fig. 25 Cyclic E-log i polarization curve for Incoloy 800 alloy in molten nitrate system, T = 398°C, ν = 0.5 mv/sec.

Fig. 26 Cyclic E-log i polarization curve for Incoloy 800 alloy in molten nitrate system, T = 547°C, ν = 0.2 mv/sec.

Fig. 27 E-log i anodic polarization curves for Incoloy 800 alloy in molten nitrate system at different concentration of added K_2CrO_4: (a) 0, (b) 0.001, (c) 0.006, (d) 0.010 M, T = 547°C, ν = 0.2 mv/sec. Dotted lines represents the reverse scan for experiment (d).

Fig. 1

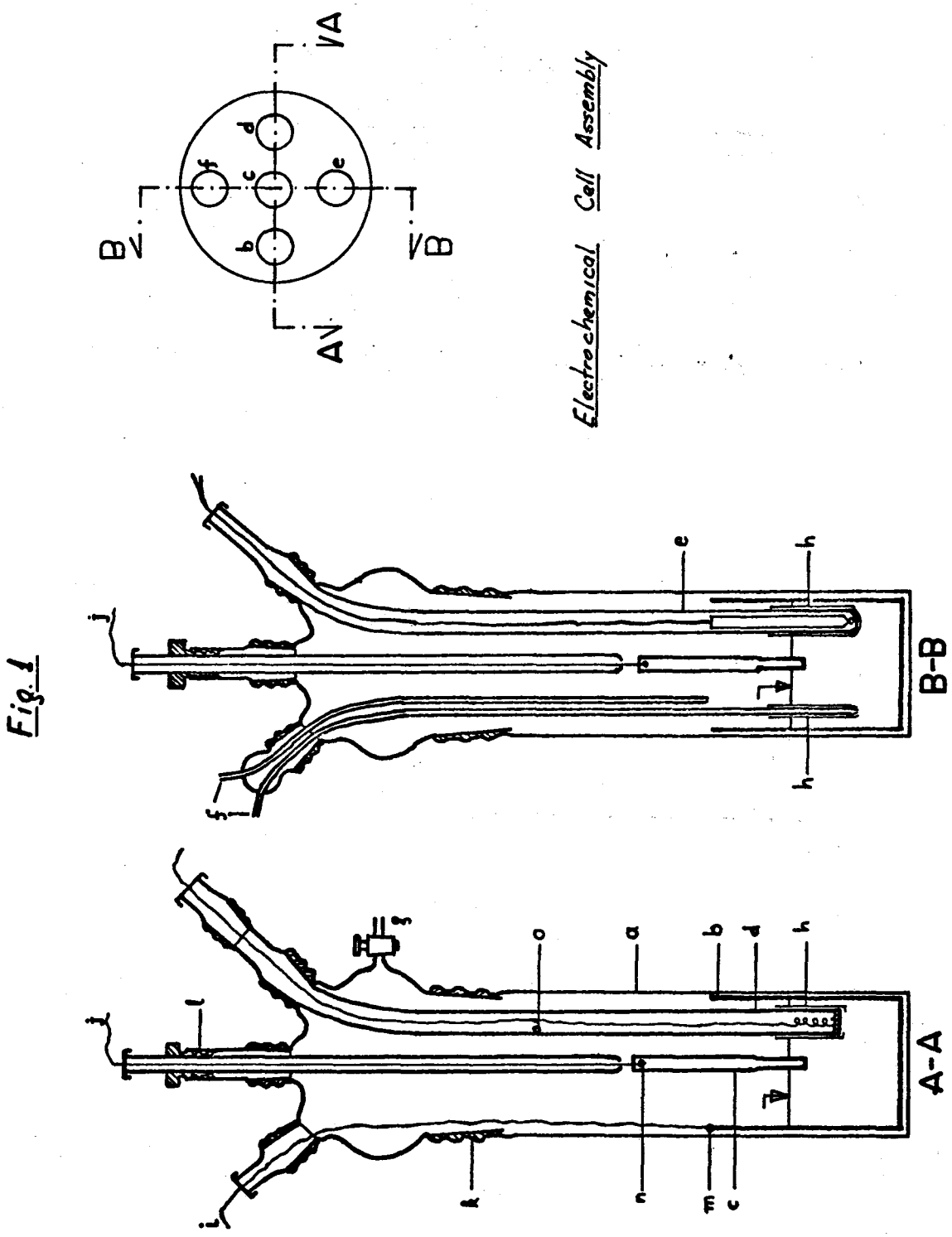

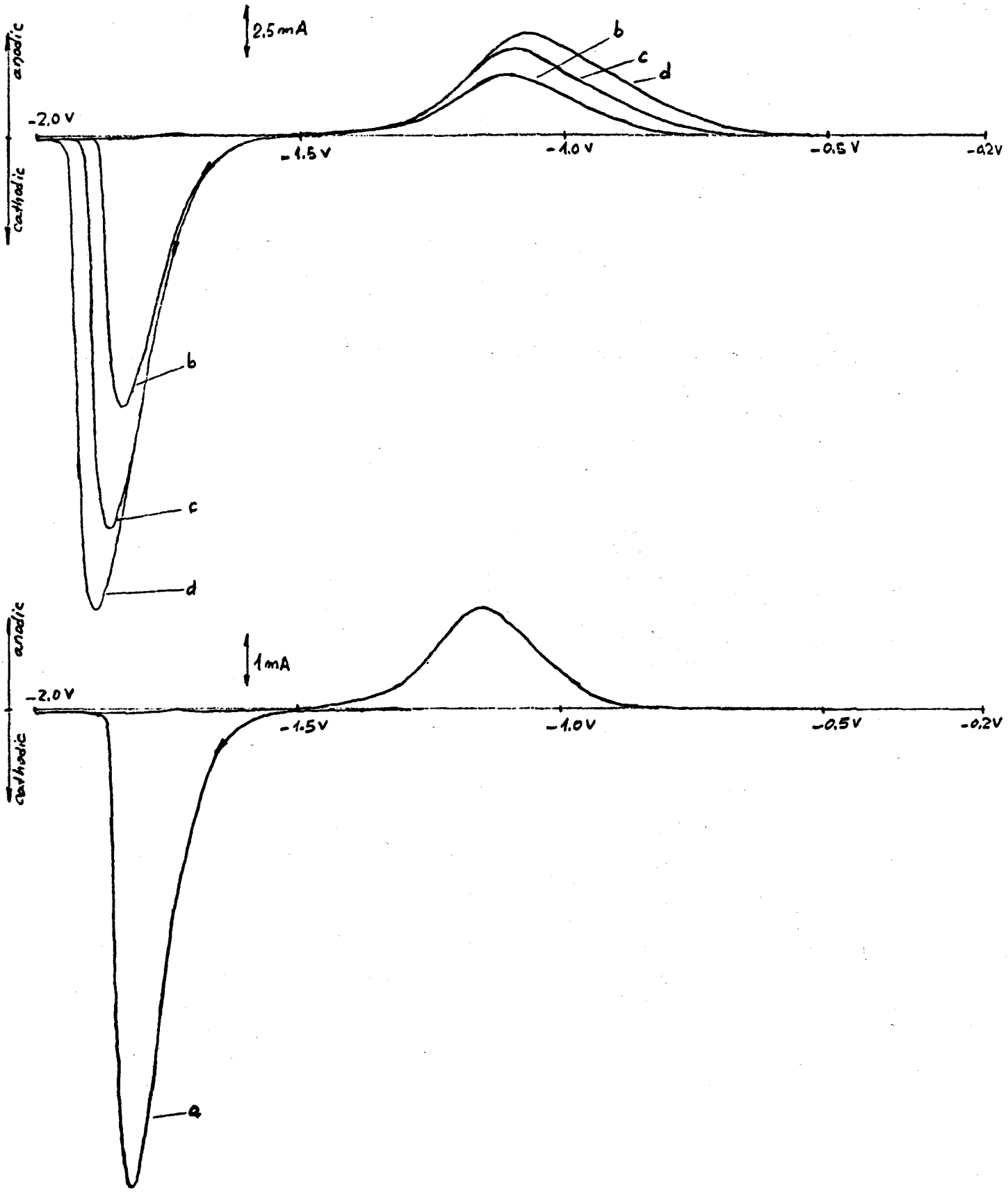
2,5 mA
anodic
cathodic
-2.0 V
-1.5 V
-1.0 V
-0.5 V
-0.2V
b
c
d
b
c
d
1 mA
anodic
cathodic
-2.0 V
-1.5 V
-1.0 V
-0.5 V
-0.2V
a

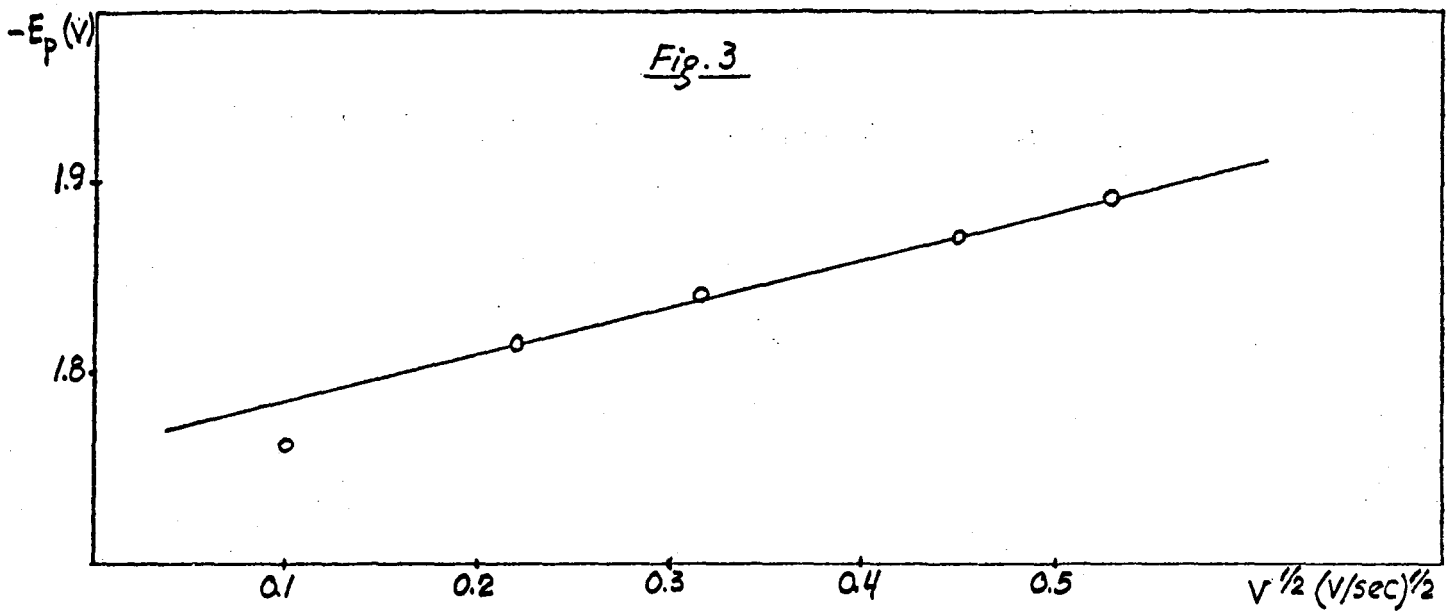
$-E_p$ (V)
1.9
1.8
0.1
0.2
0.3
0.4
0.5
V 1/2 (V/sec)1/2

Fig. 3

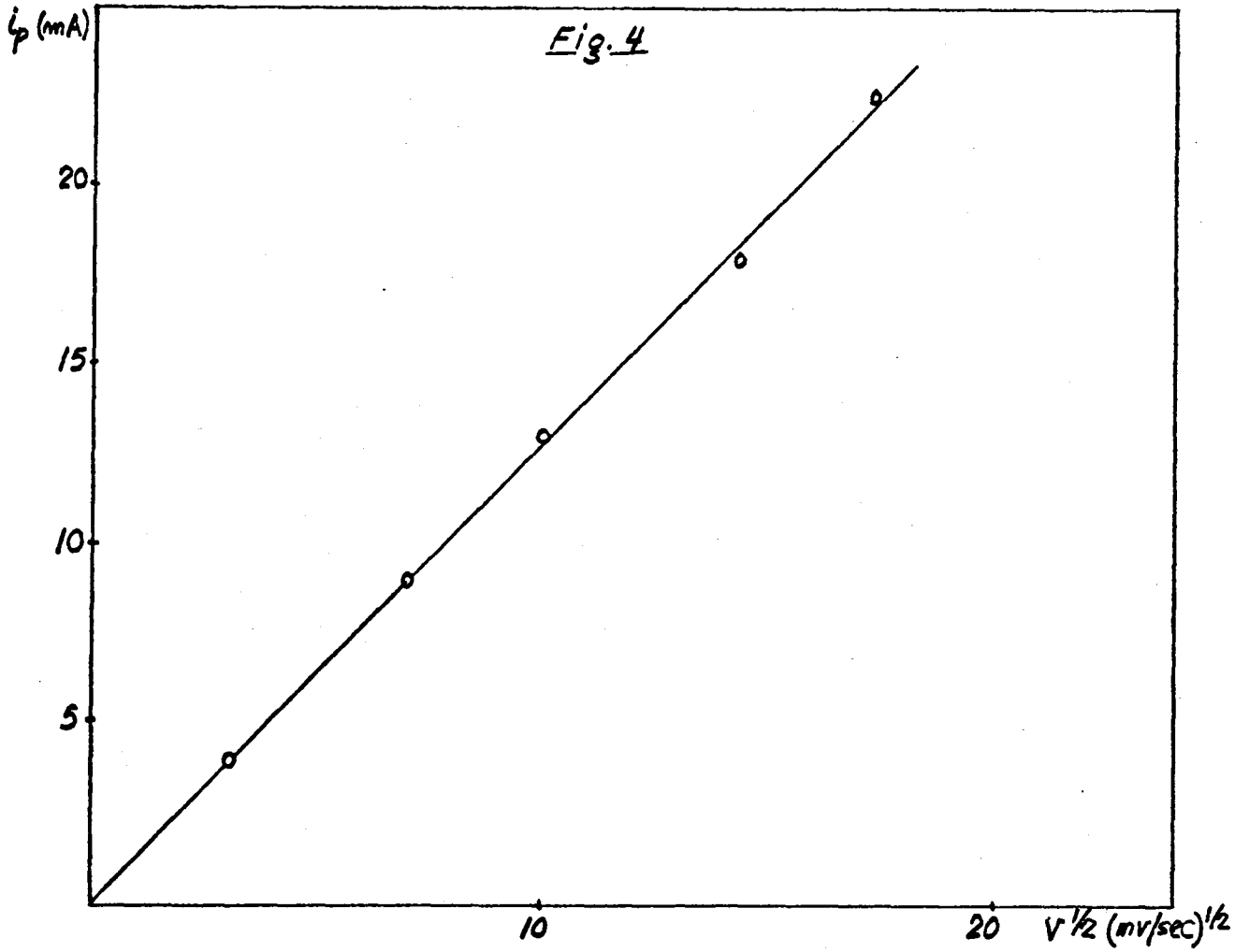
i_p (mA)
20
15
10
5
10
20
V 1/2 (mv/sec)1/2

Fig. 4

Fig. 5

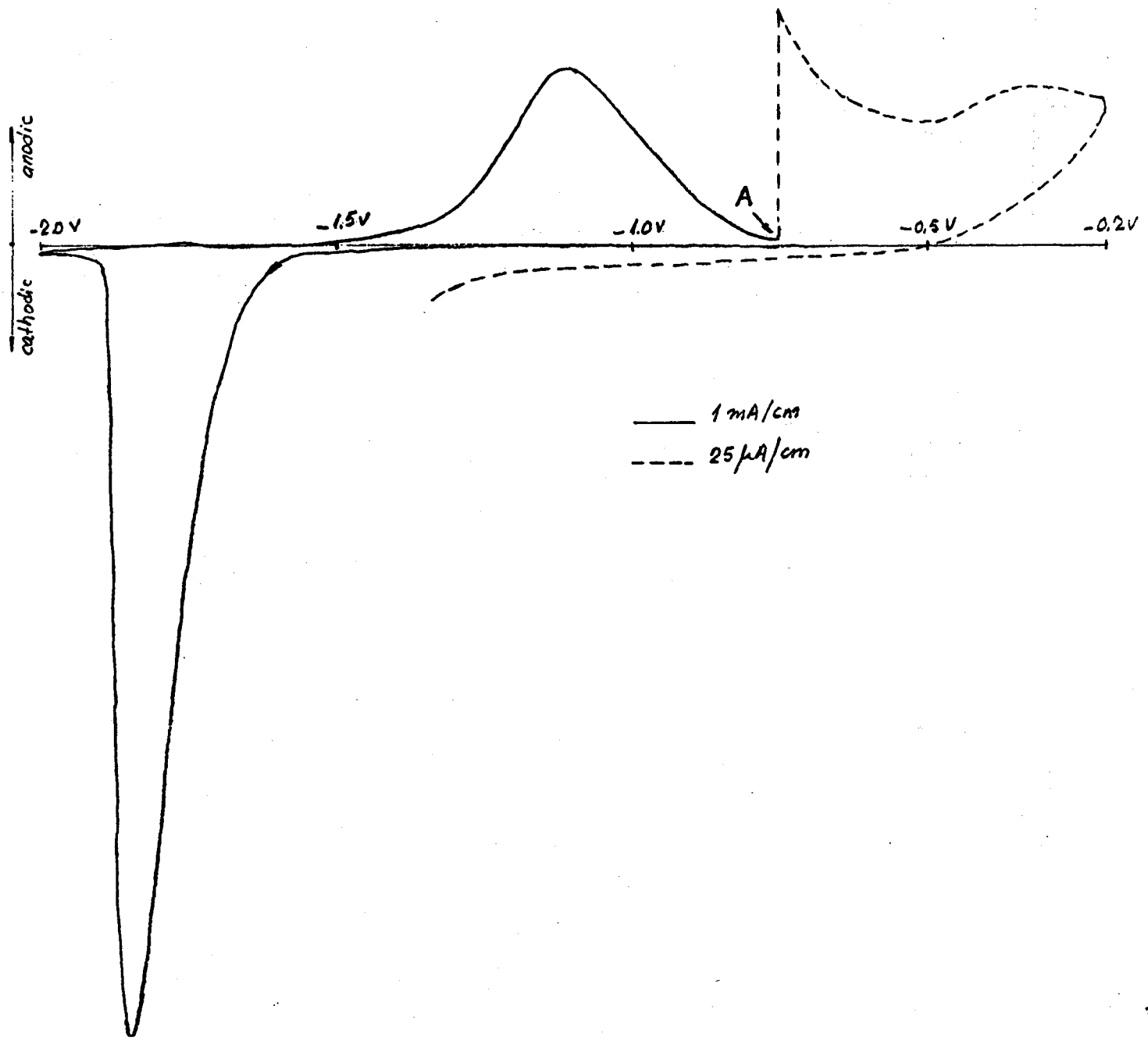

Fig. 6

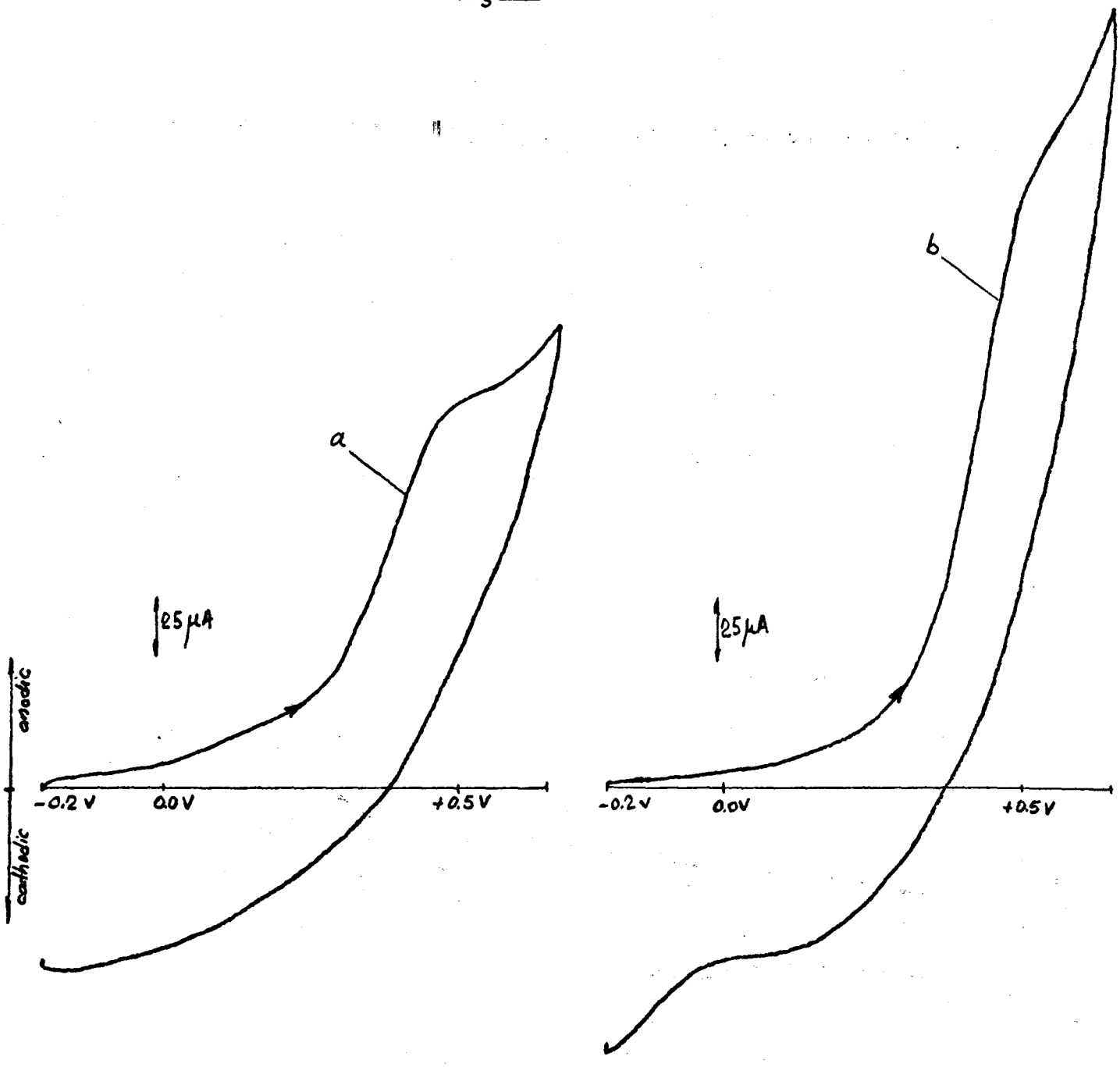

Fig. 7

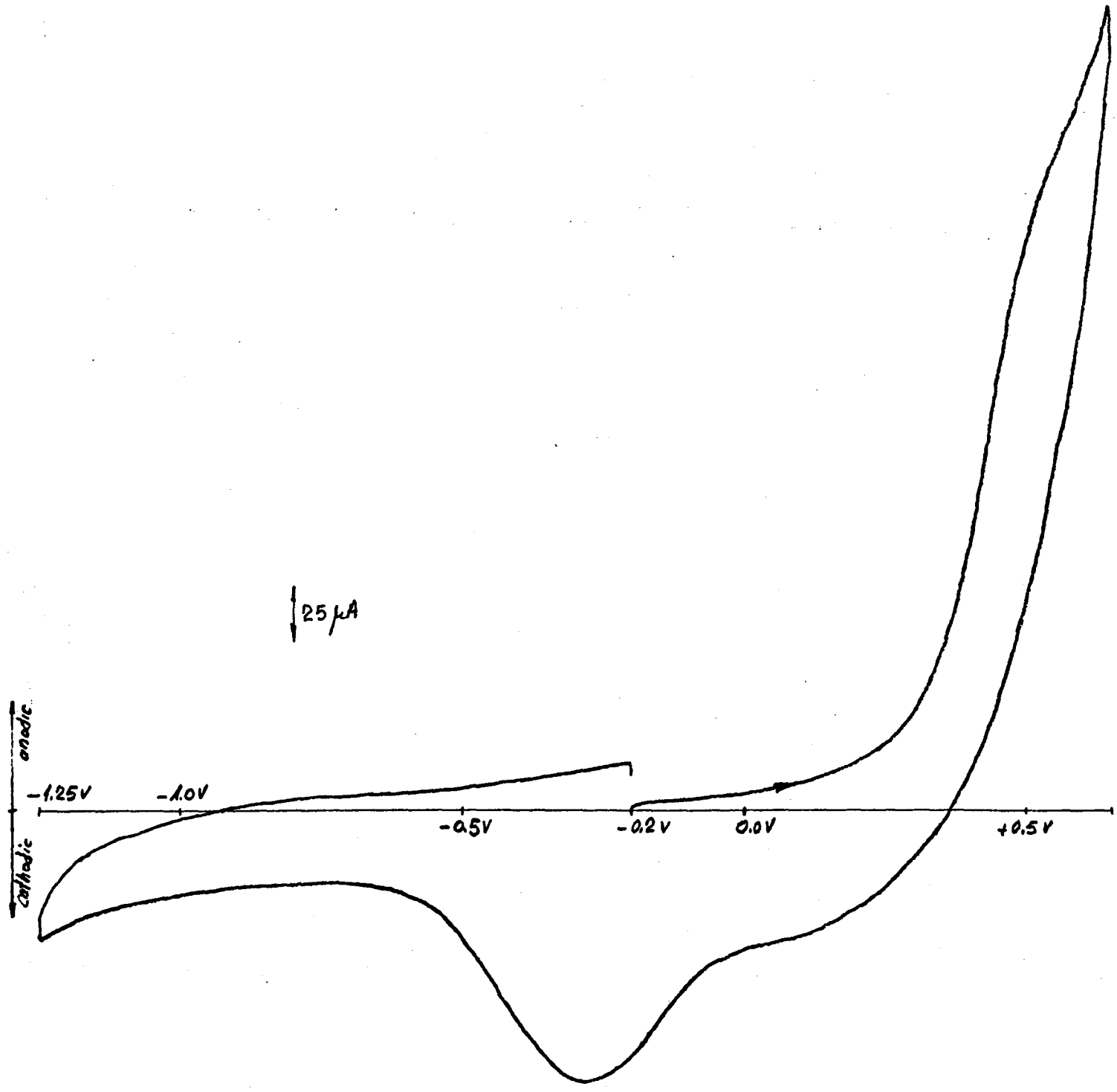

Fig. 8

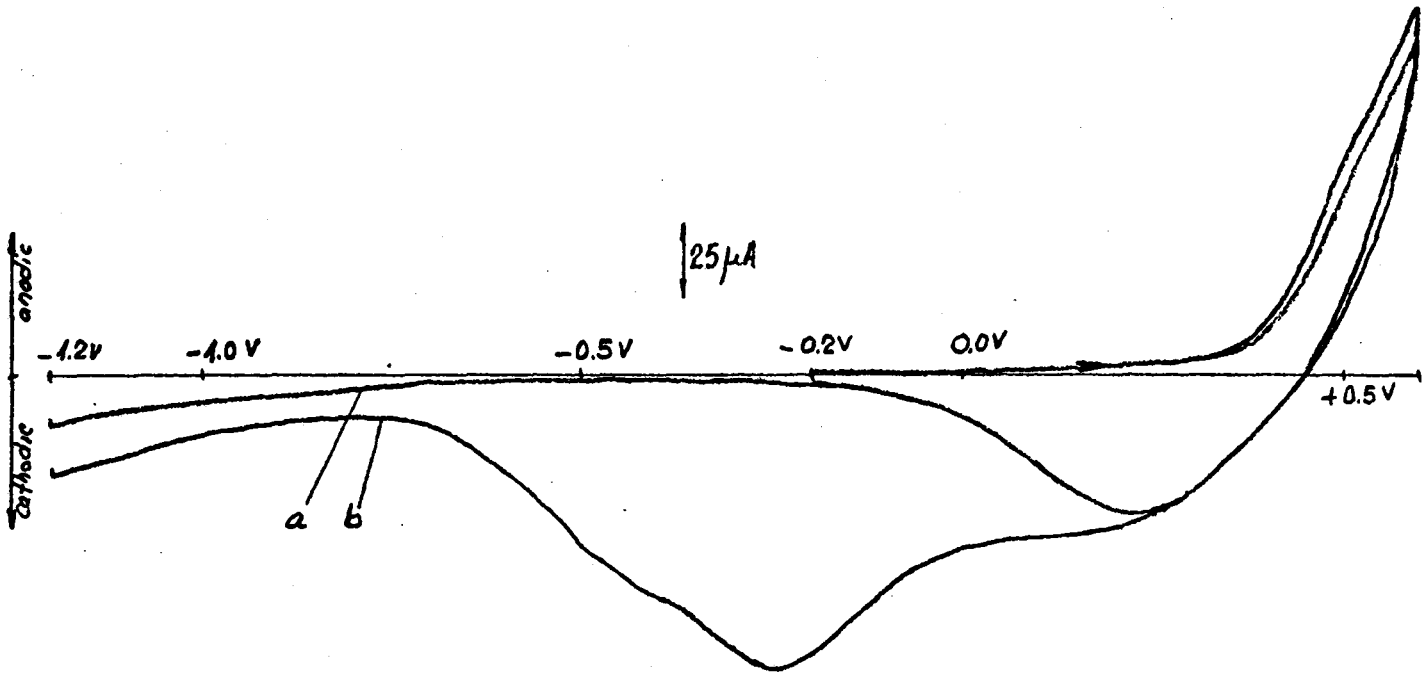

Fig. 9

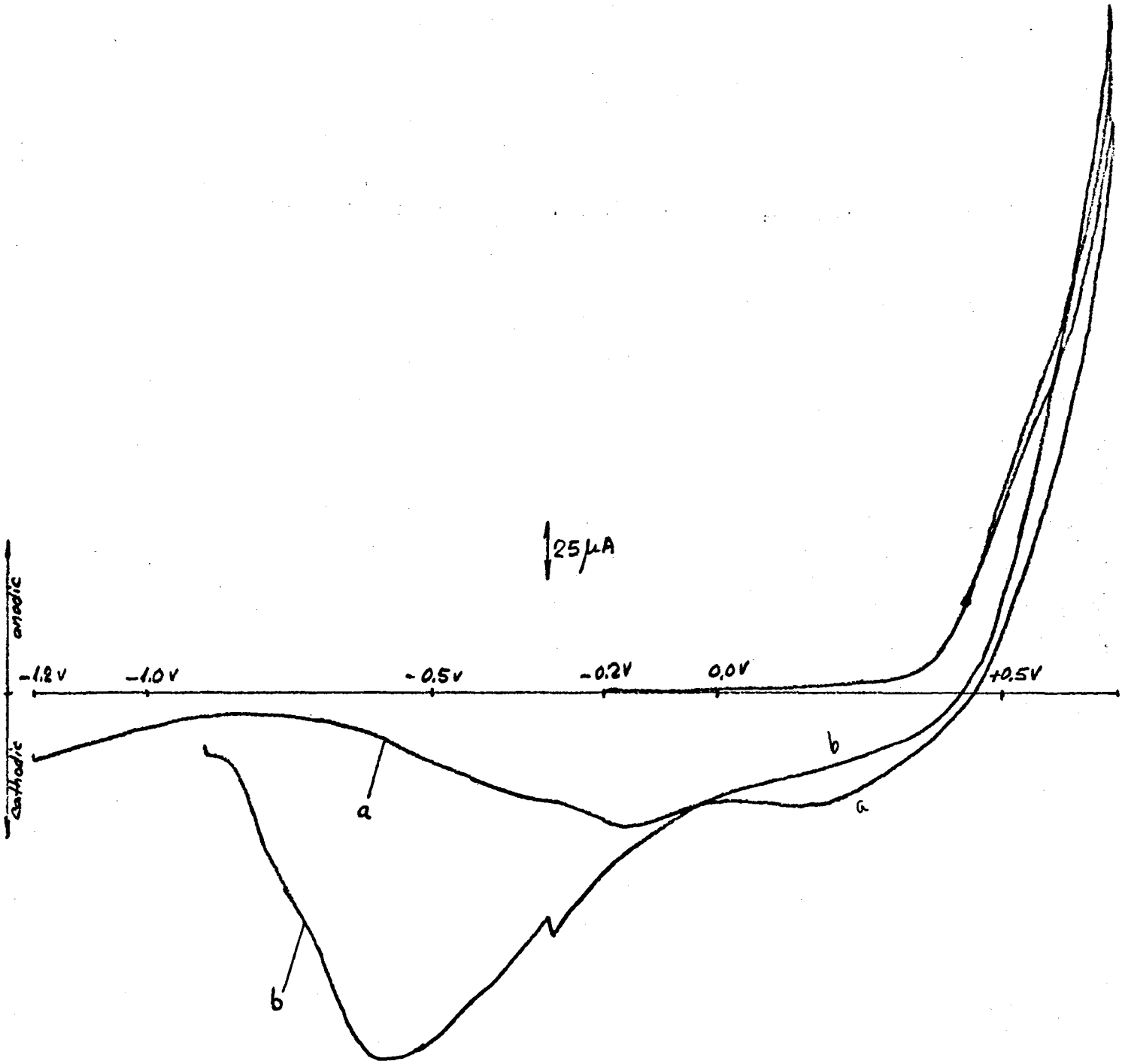

Fig. 10

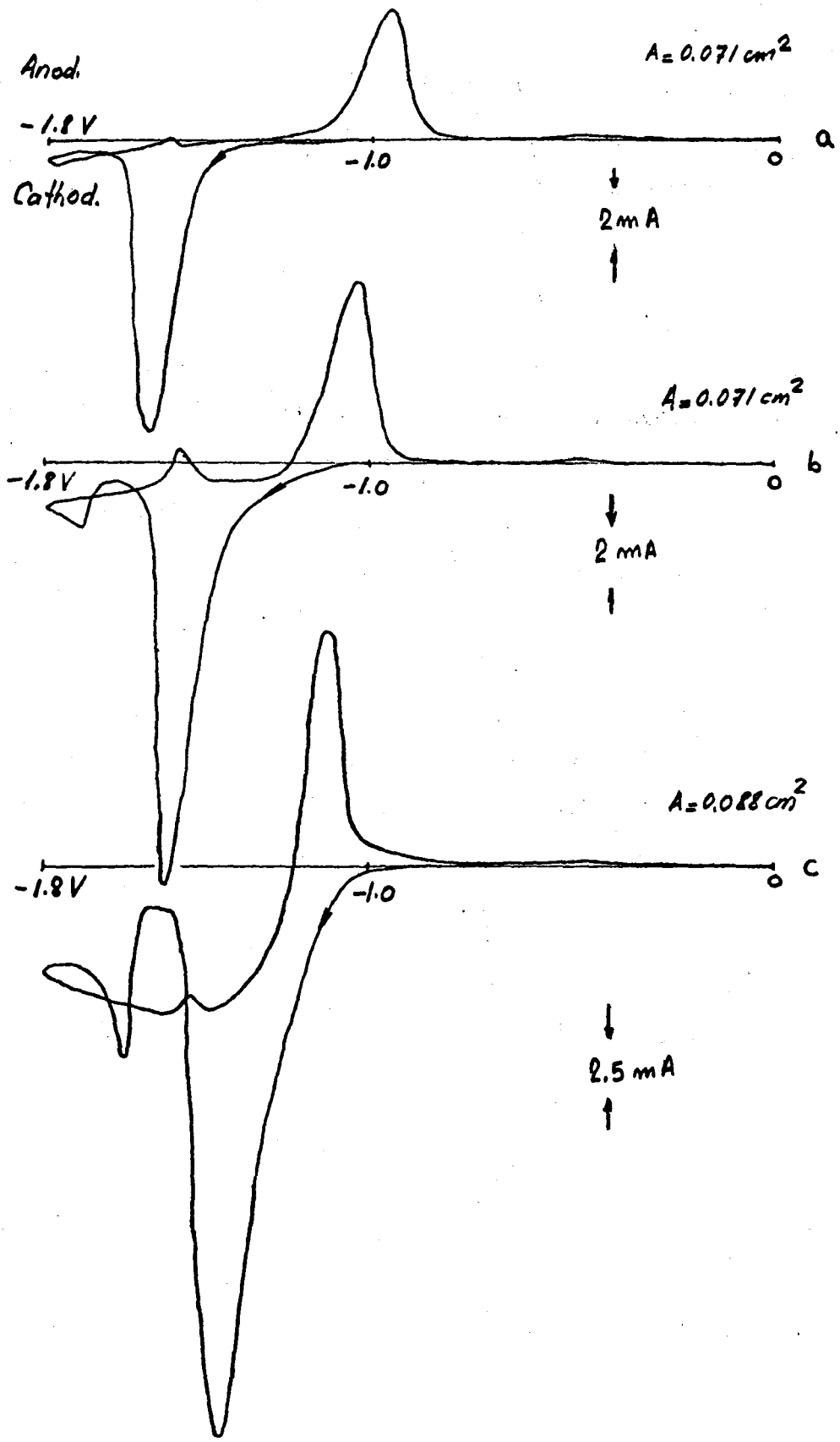
Anod.
-1.8 V
-1.0
0
Cathod.
A = 0.071 cm²
a
2 mA
A = 0.071 cm²
-1.8 V
-1.0
0
b
2 mA
A = 0.088 cm²
-1.8 V
-1.0
0
c
2.5 mA

Fig. 10 (cont.)

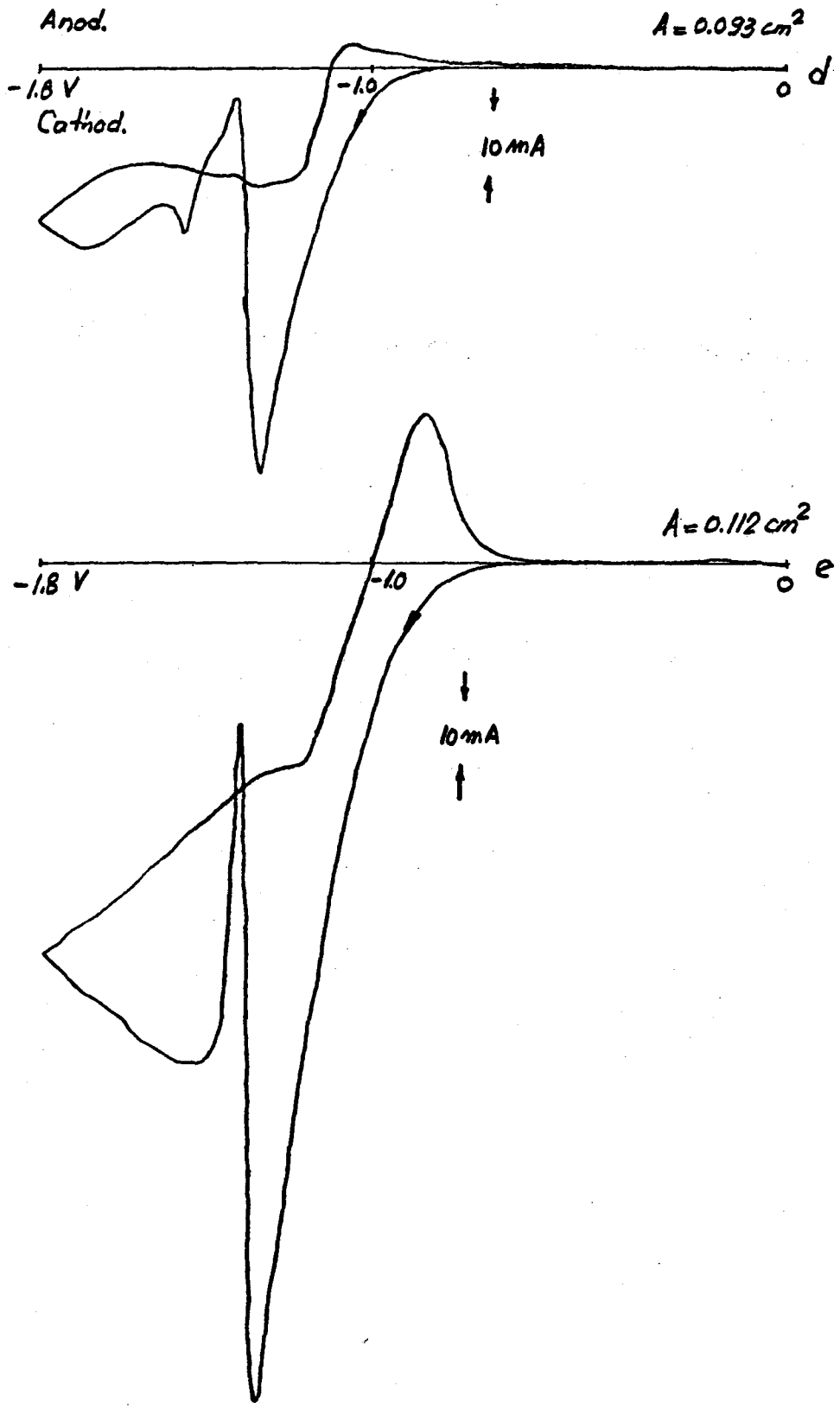

Fig. 10 (cont.)

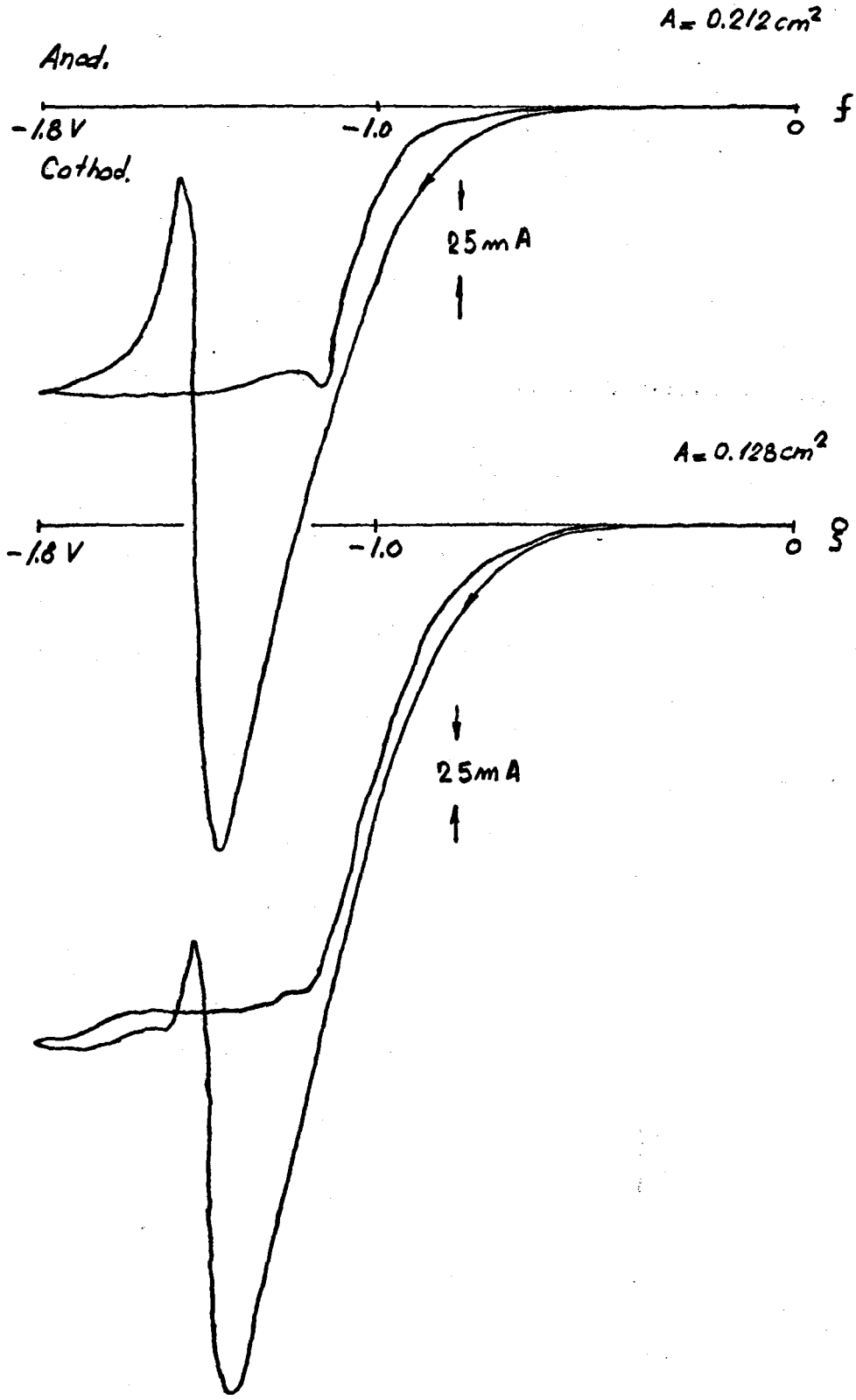

Fig. 11

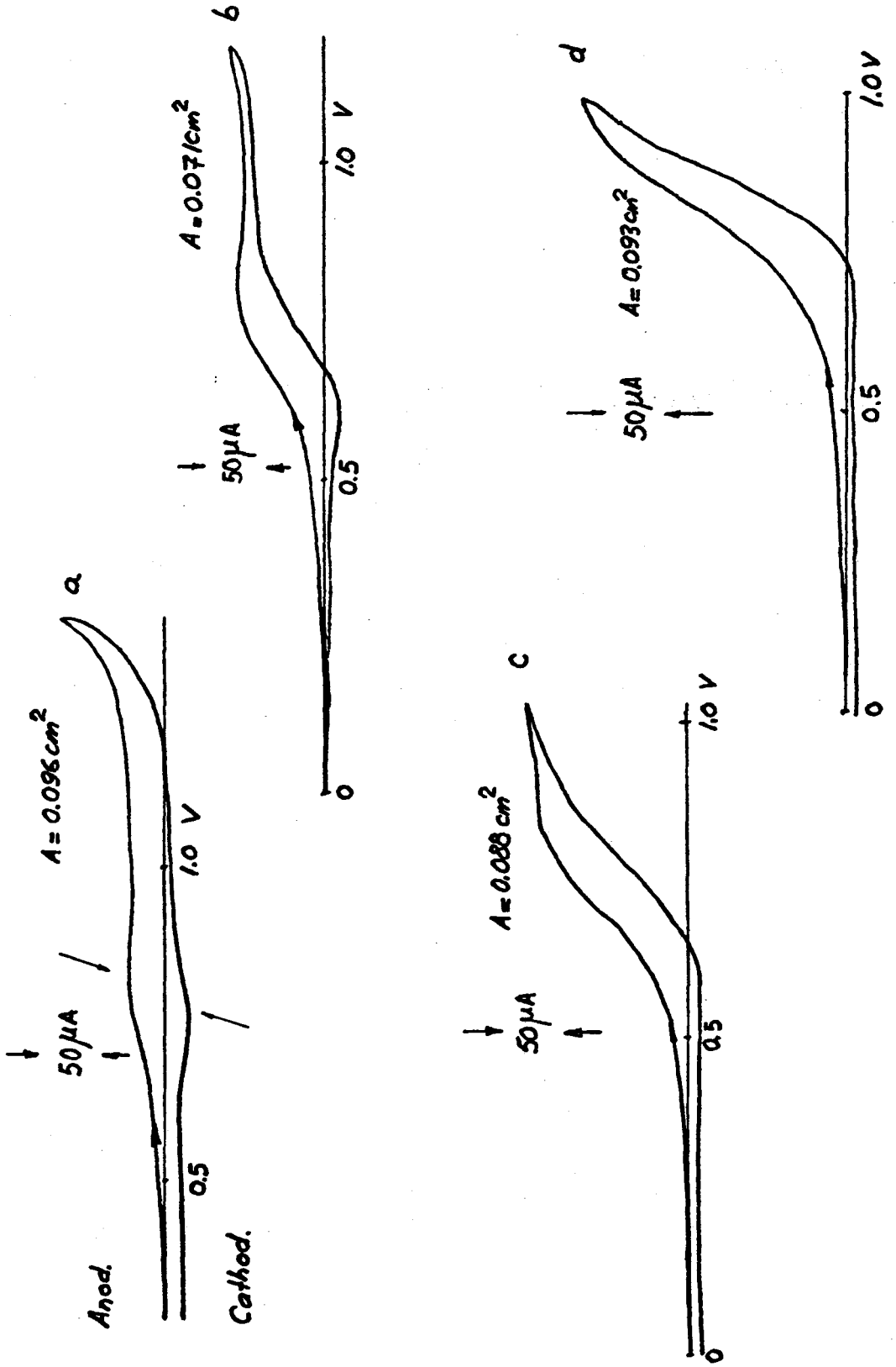
a
A = 0.096 cm²
50 µA
1.0 V
0.5
Anod.
Cathod.
b
A = 0.07 cm²
50 µA
1.0 V
0.5
0
c
A = 0.088 cm²
50 µA
1.0 V
0.5
0
d
A = 0.093 cm²
50 µA
1.0 V
0.5
0

Fig. 11 (cont.)

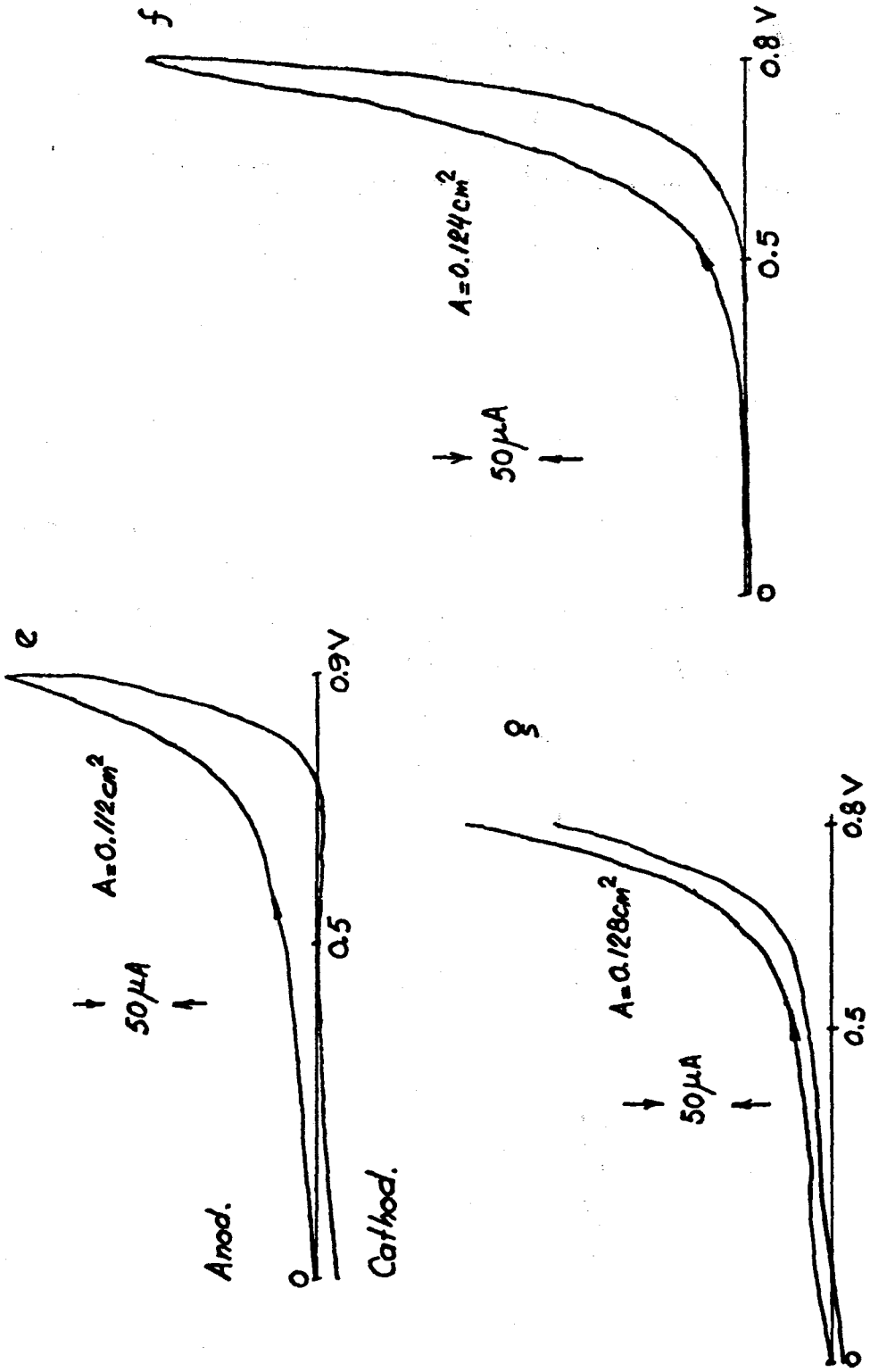
e
A=0.112cm²
50μA
0.5
0.9V
0
Anod.
Cathod.
f
A=0.124cm²
50μA
0.5
0.8 V
0
g
A=0.128cm²
50μA
0.5
0.8V
0

Fig. 12

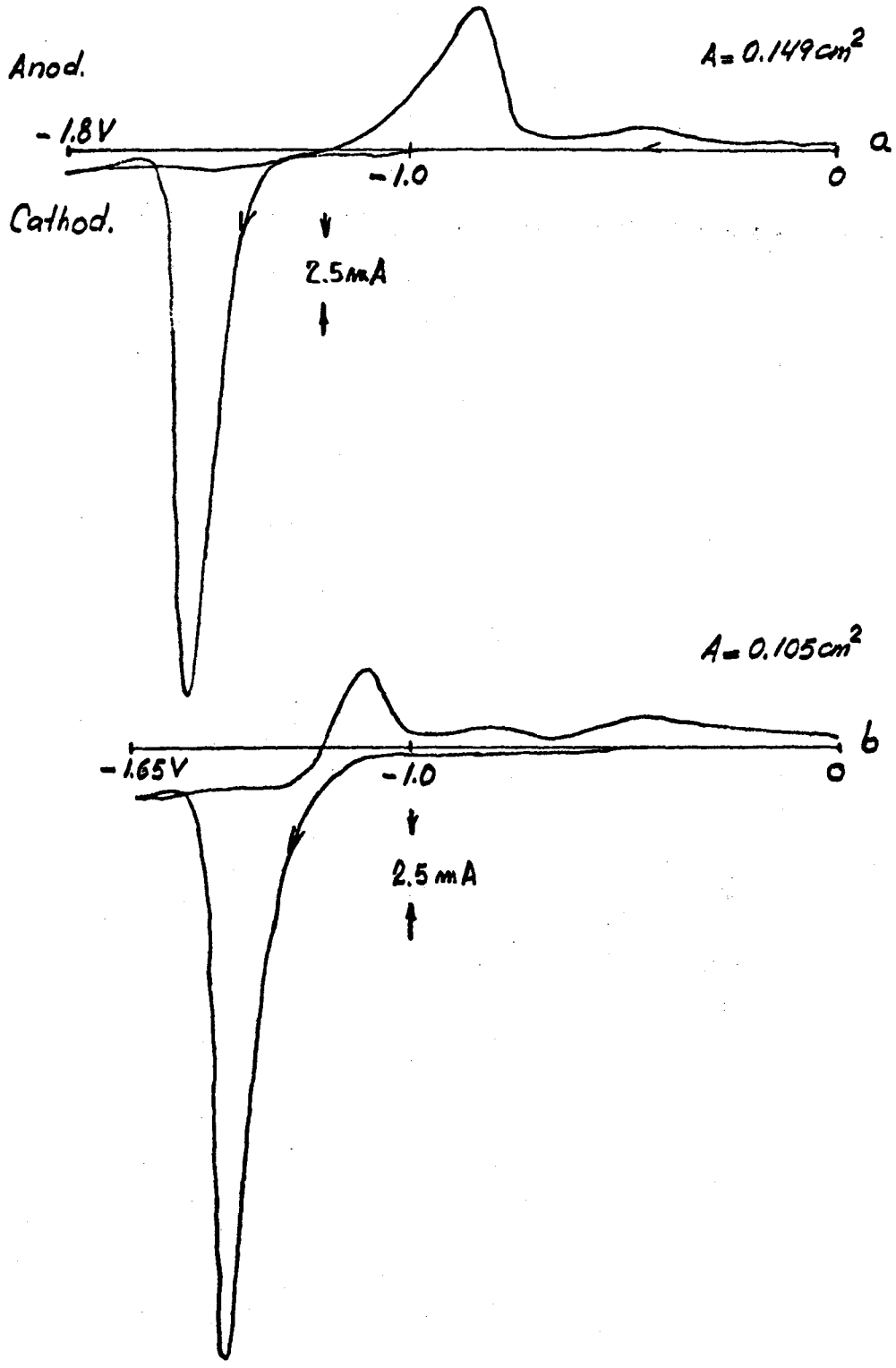

Fig. 12 (cont.)

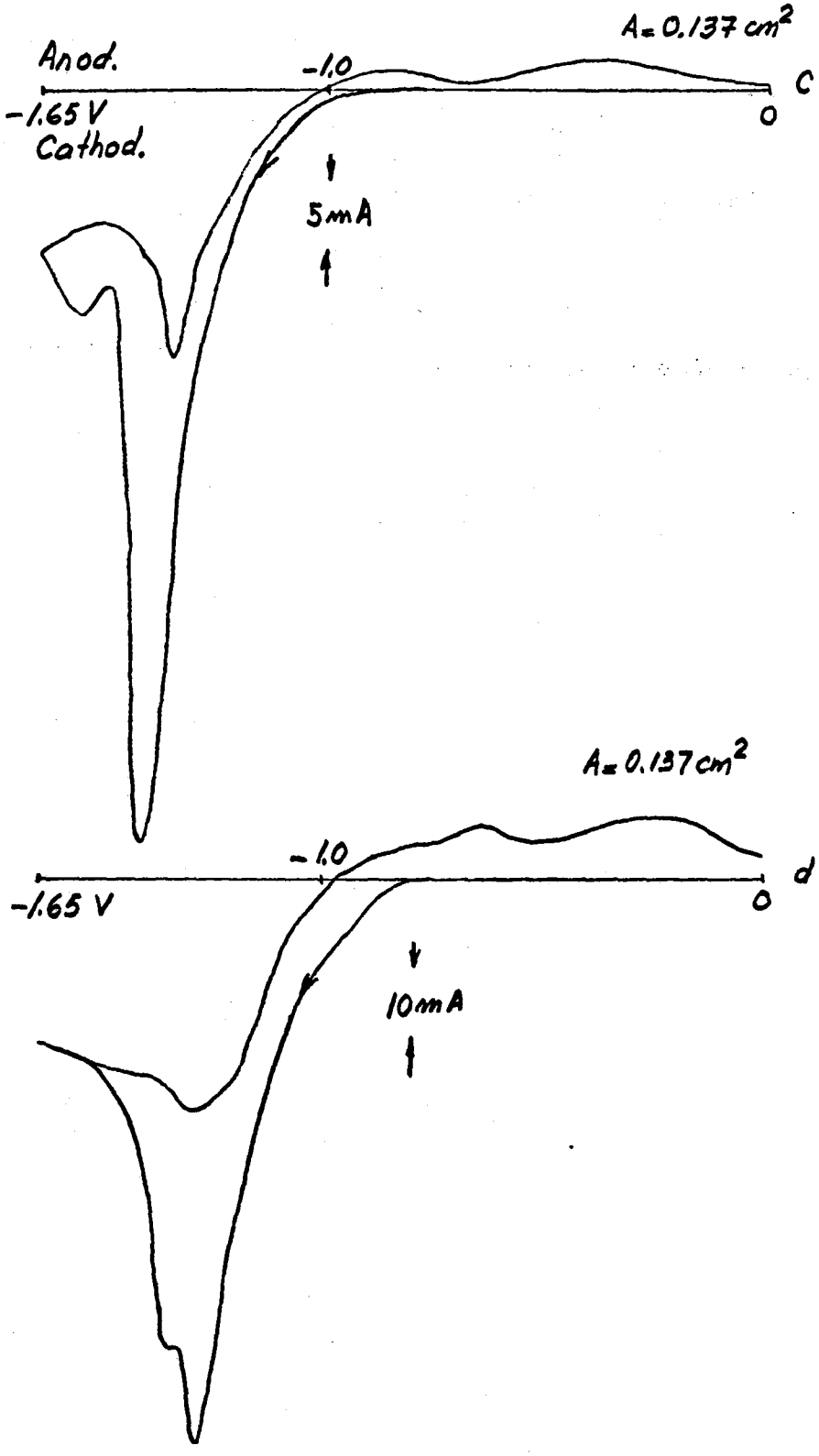

Fig. 12 (cont.)

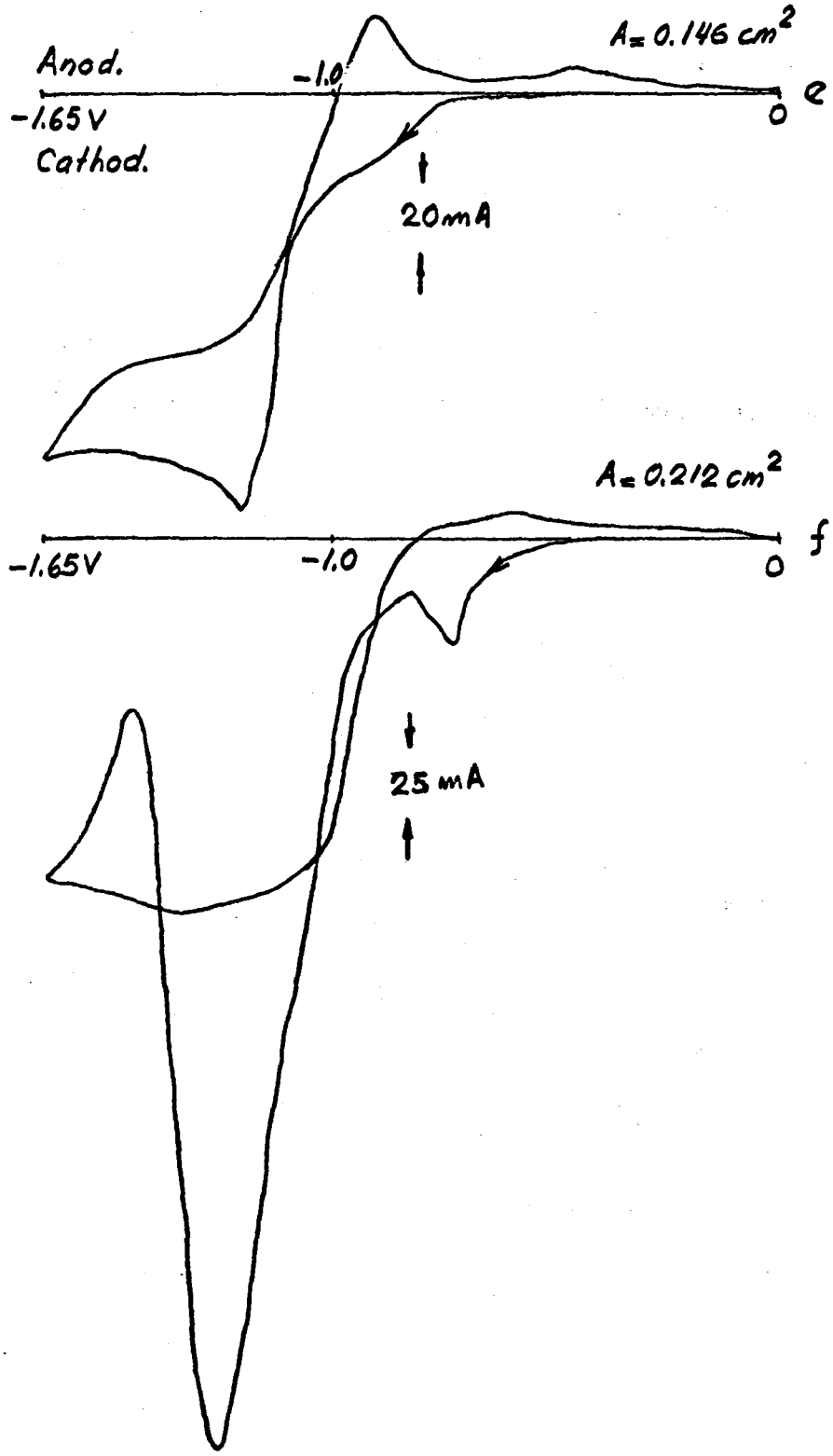
A= 0.146 cm²
Anod.
-1.0
-1.65 V
Cathod.
0
e
20 mA
A= 0.212 cm²
-1.65 V
-1.0
0
f
25 mA

Fig. 12 (cont.)

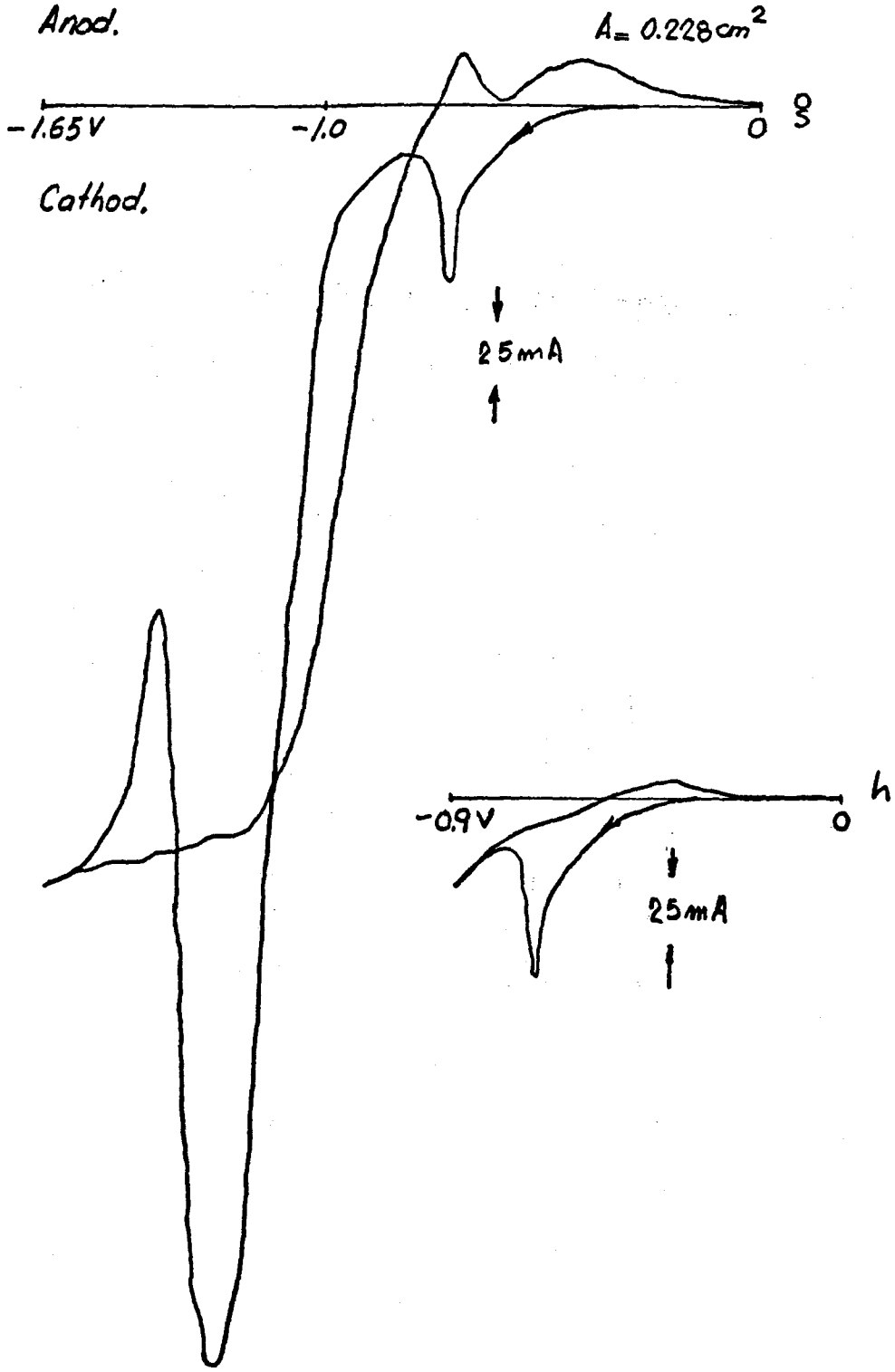

Fig. 12 (cont.)

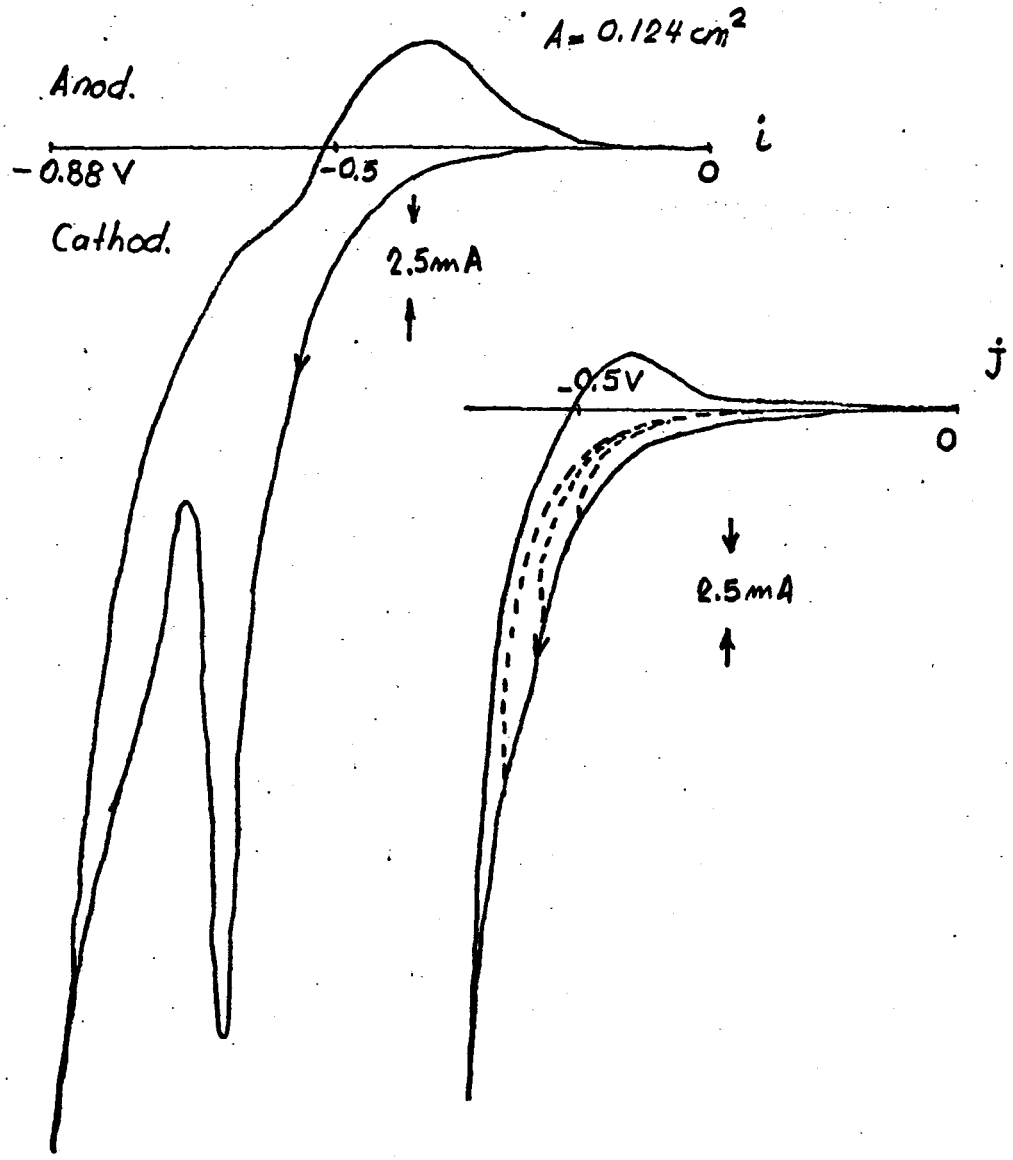

Fig. 13

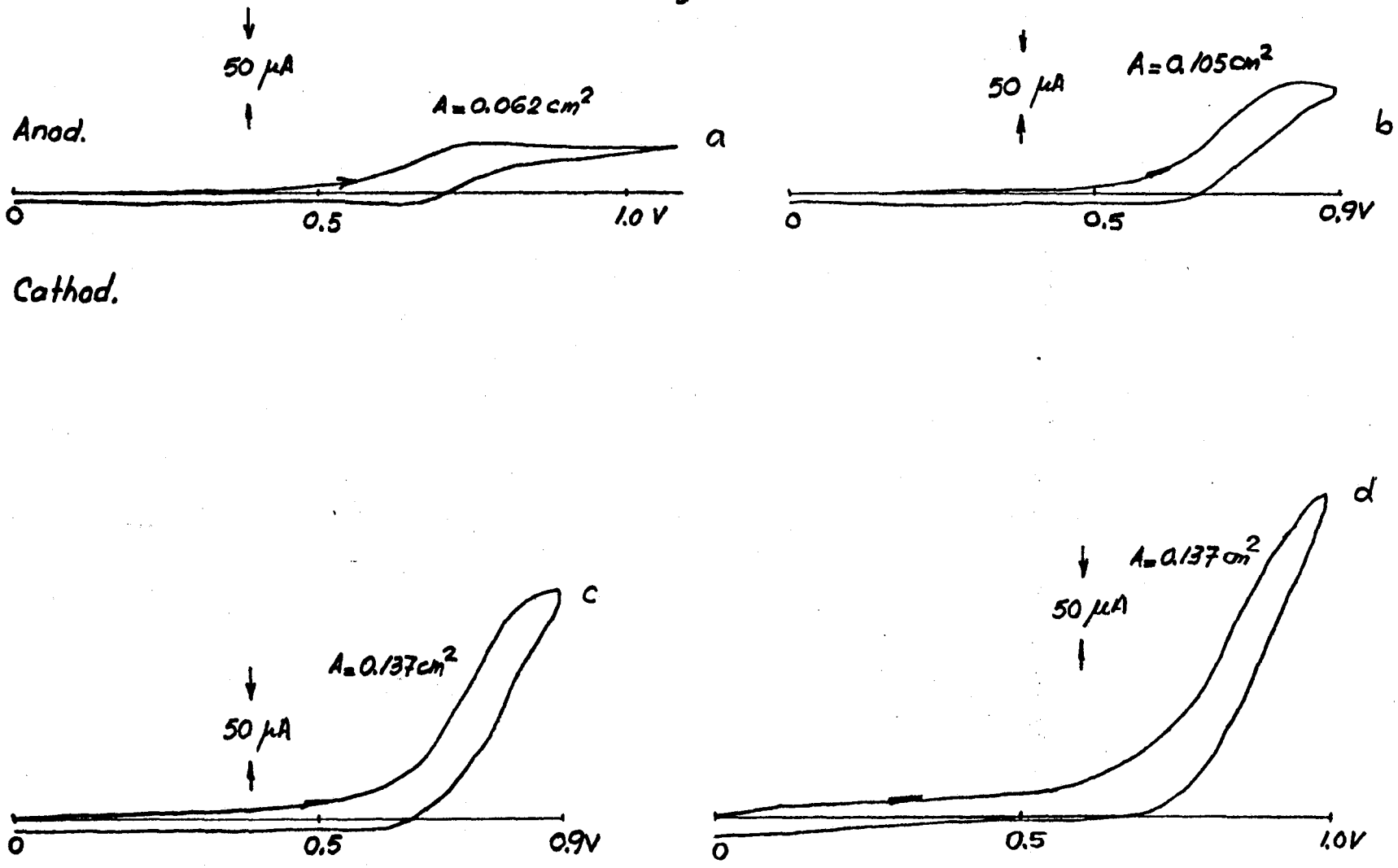
50 μA
A = 0.062 cm²
Anod.
a
0
0.5
1.0 V
50 μA
A = 0.105 cm²
b
0
0.5
0.9V
Cathod.
c
A = 0.137 cm²
50 μA
0
0.5
0.9V
d
A = 0.137 cm²
50 μA
0
0.5
1.0V

Fig. 13 (cont.)

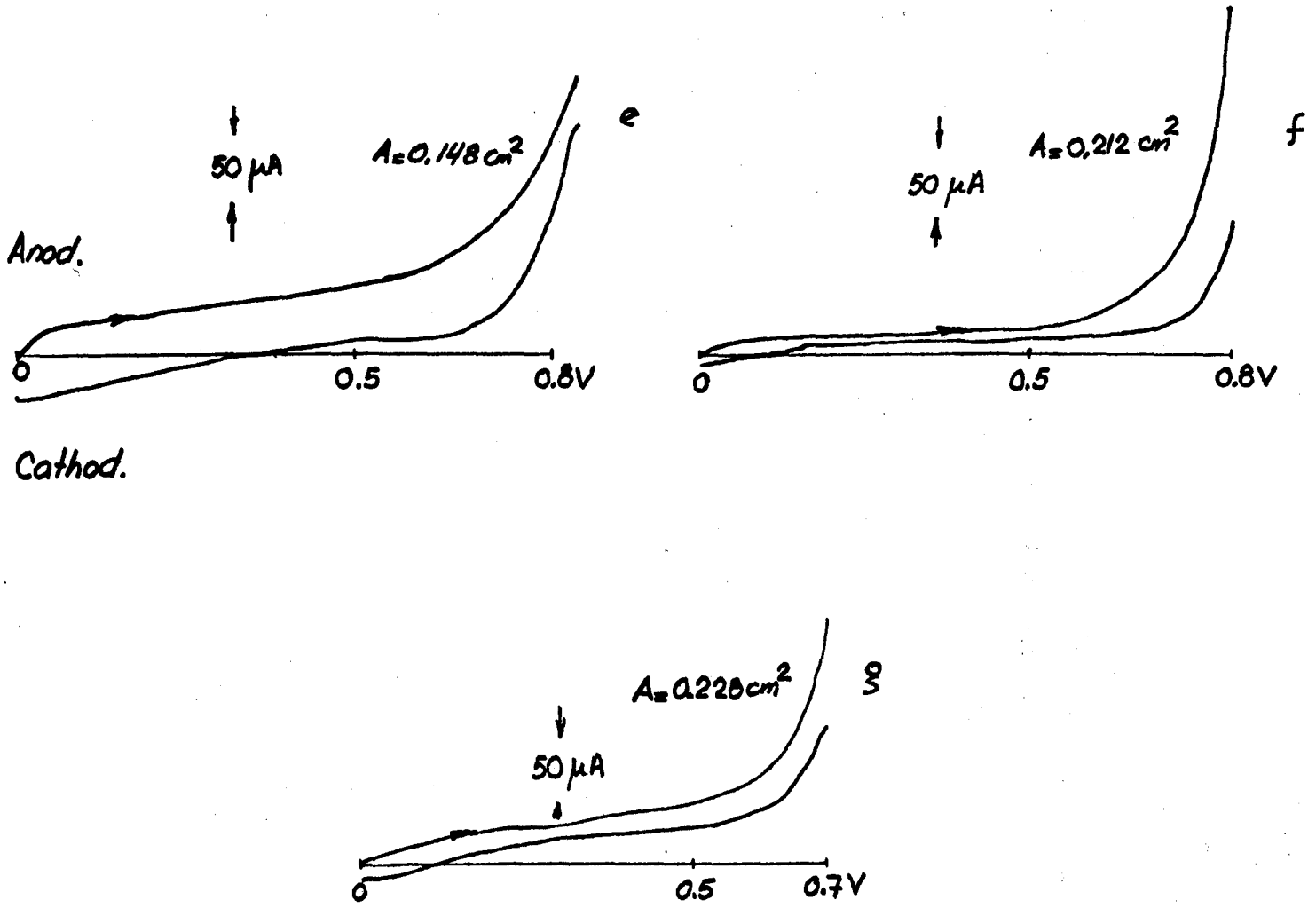
e
50 μA
A=0.148 cm²
Anod.
0
0.5
0.8V
Cathod.
f
50 μA
A=0.212 cm²
0
0.5
0.8V
g
A=0.228cm²
50 μA
0
0.5
0.7V

Fig. 14

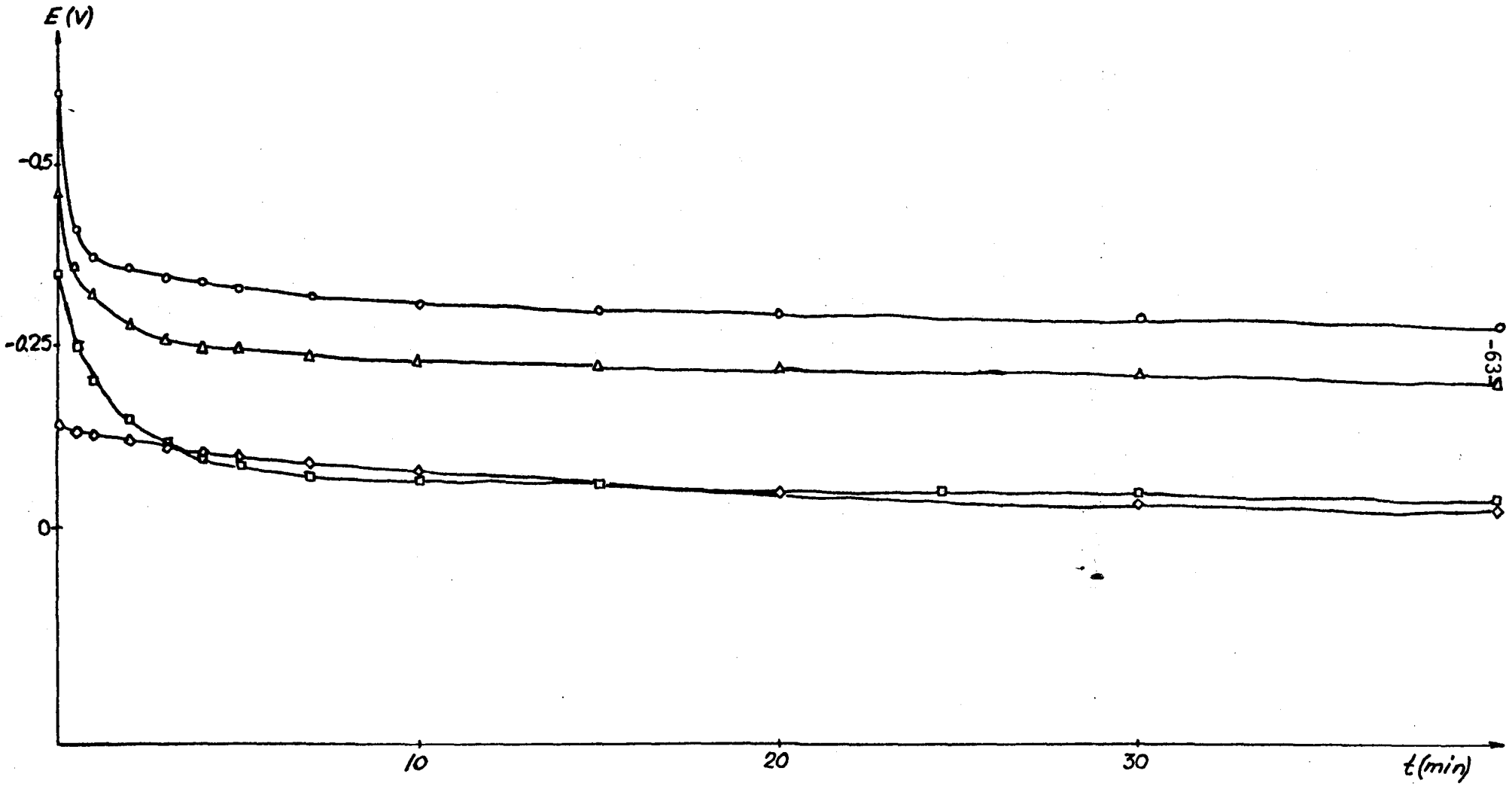

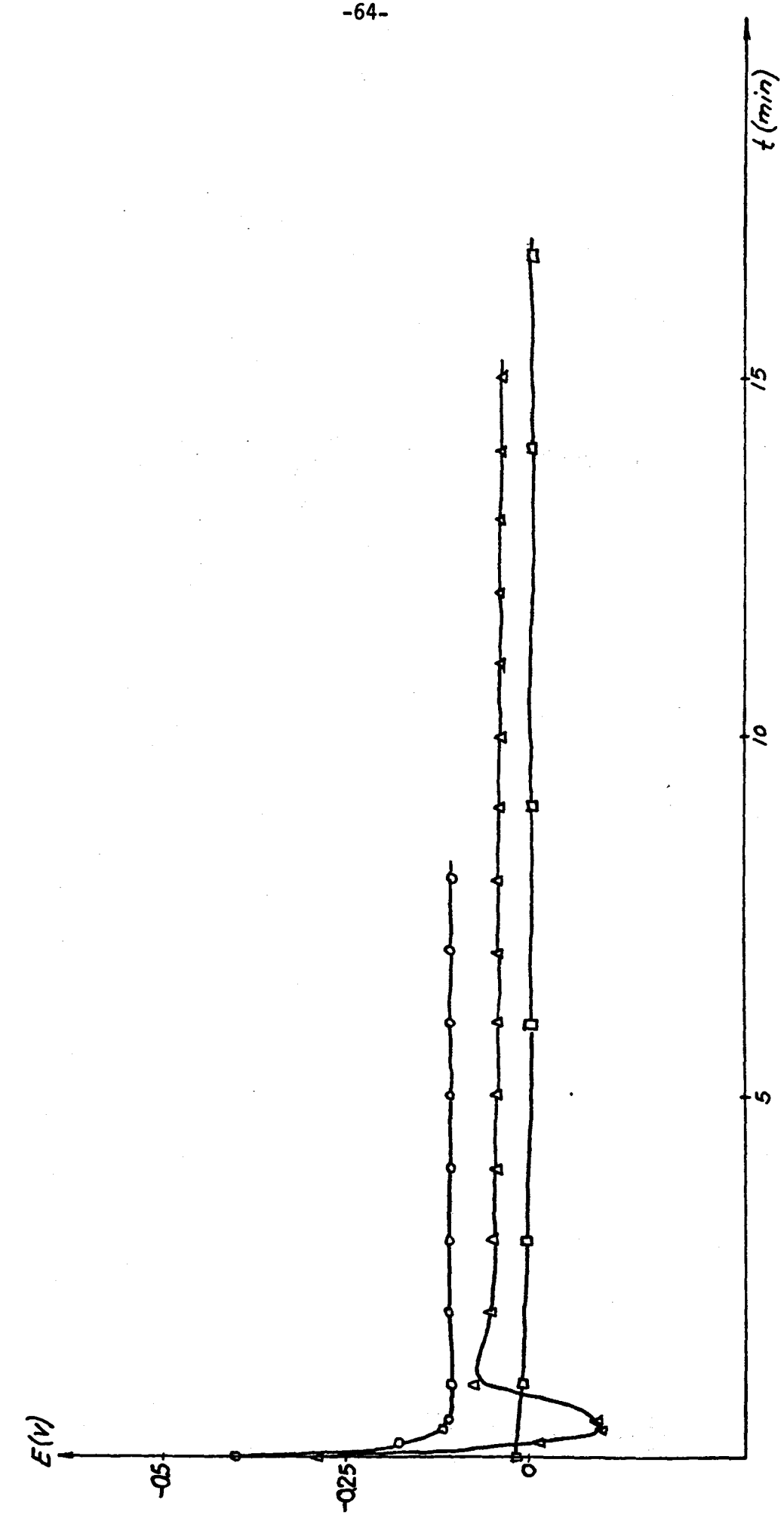

Fig. 15

Fig. 16

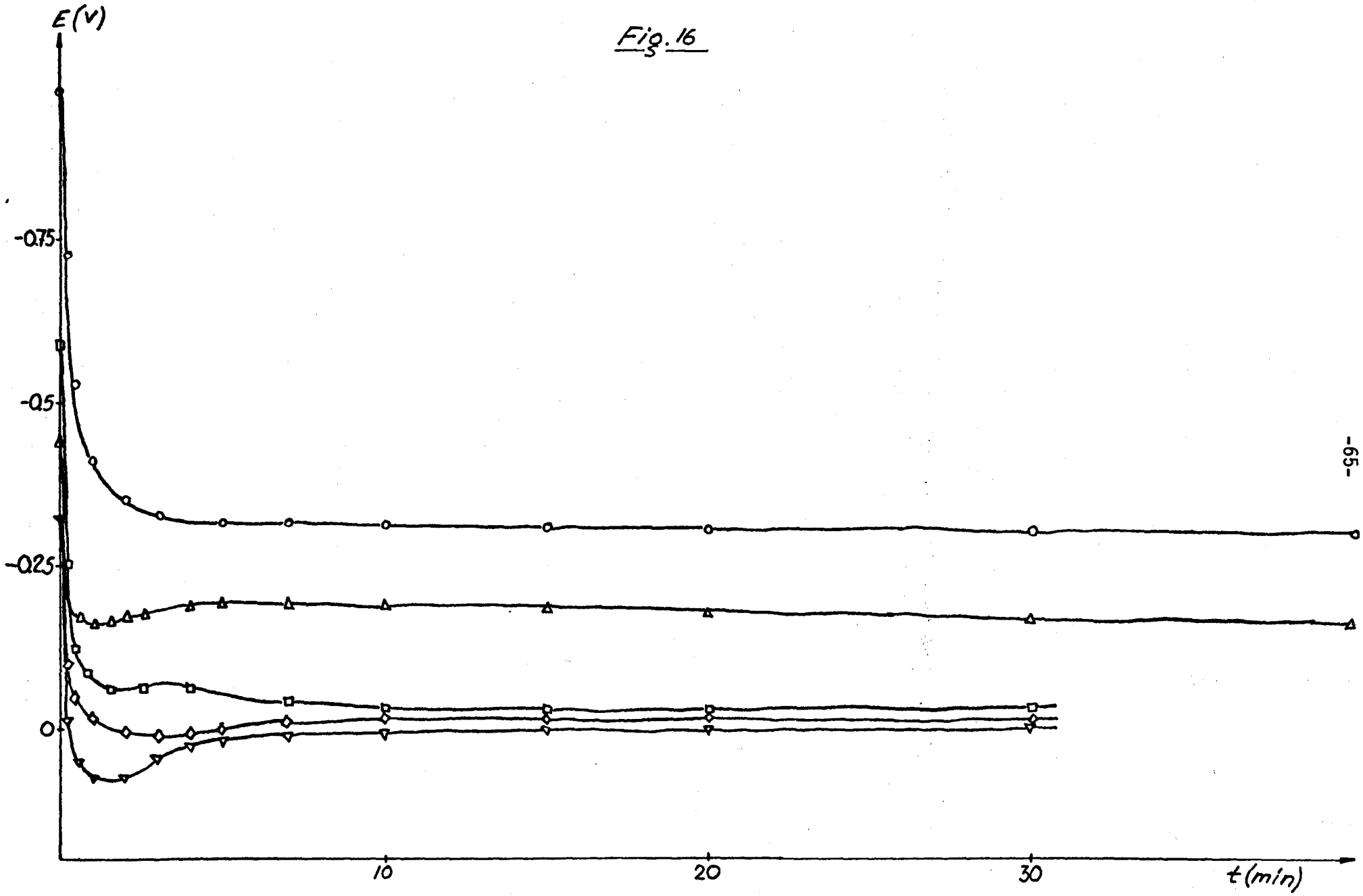

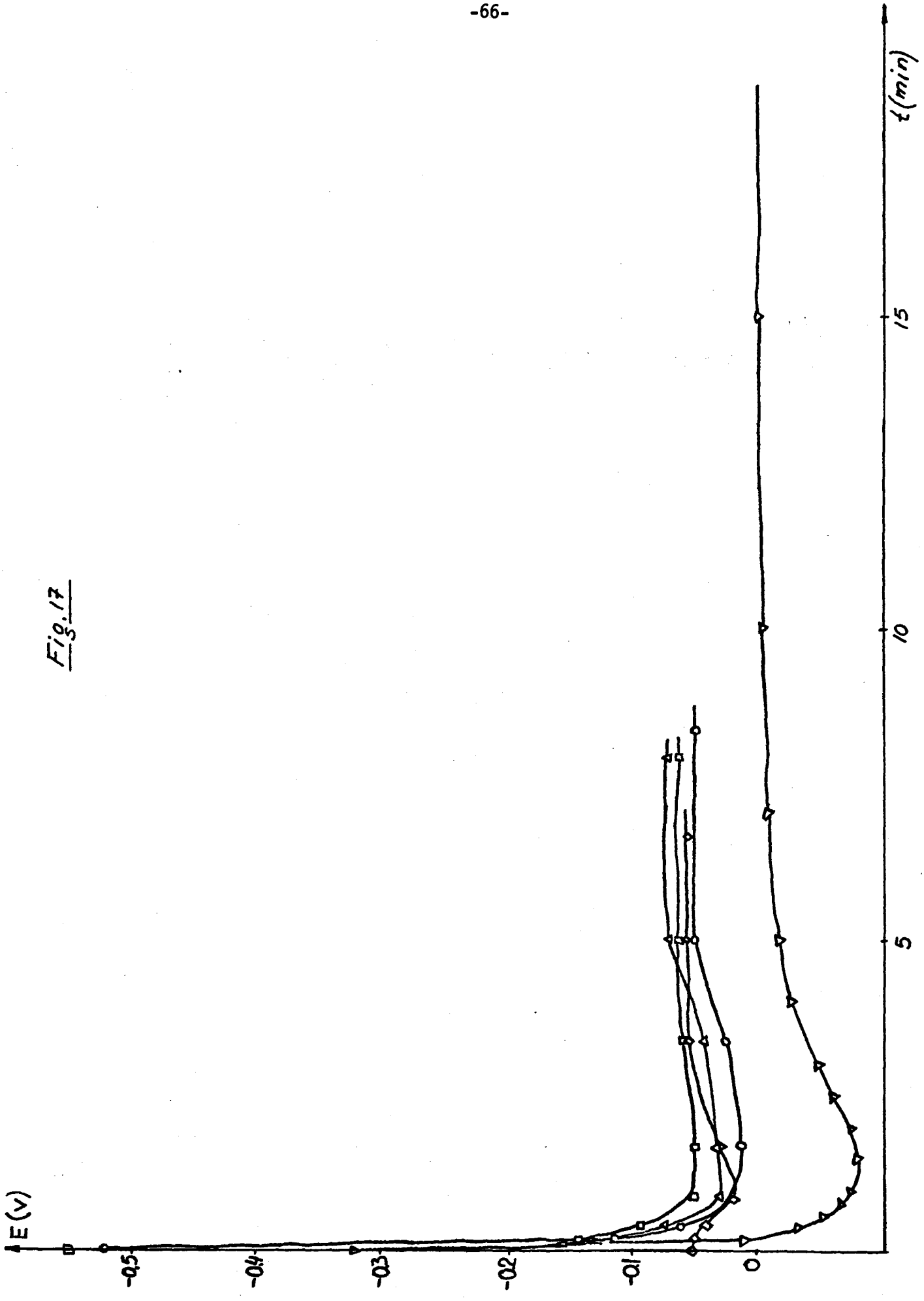

Fig. 17

Fig. 18

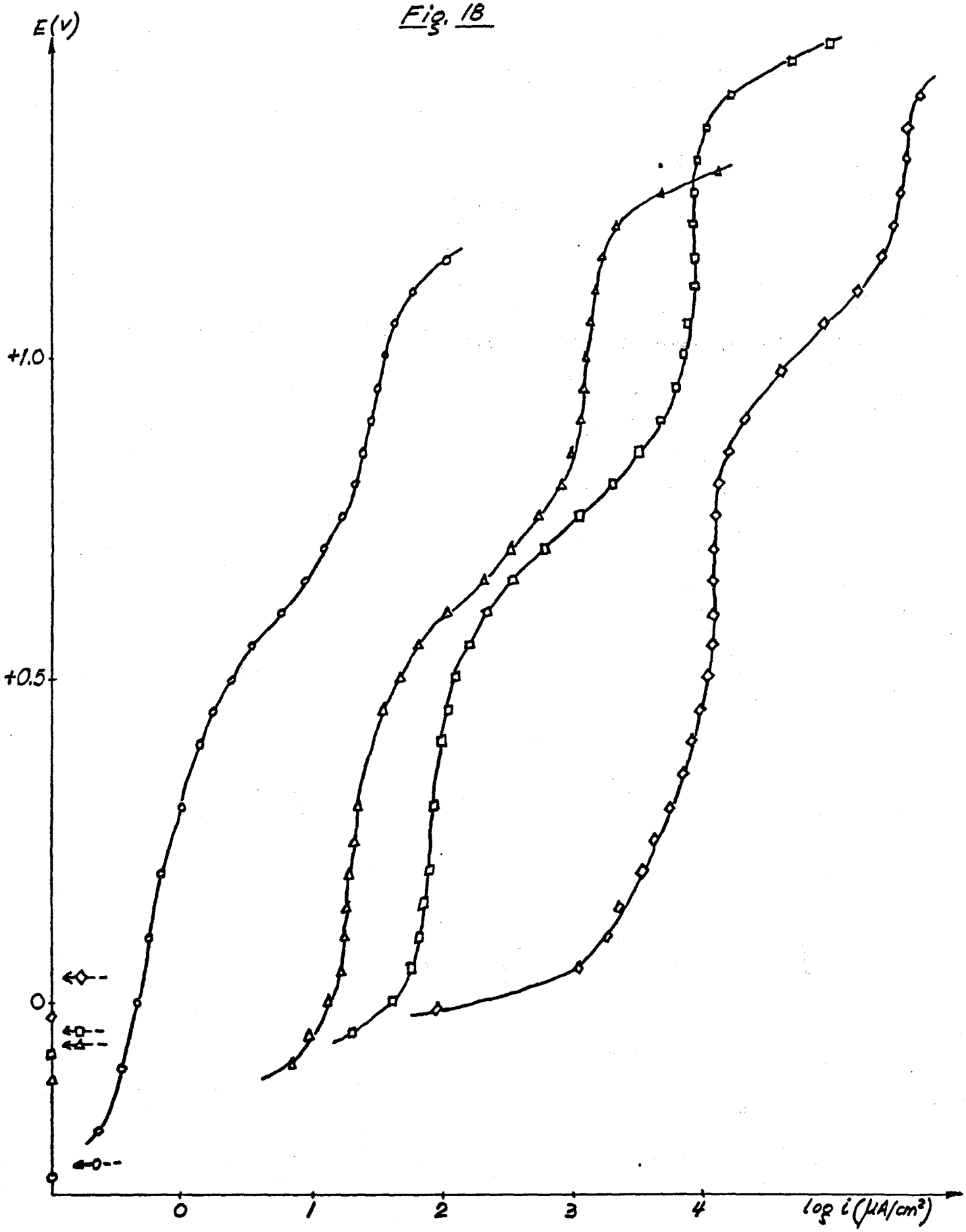

Fig. 19

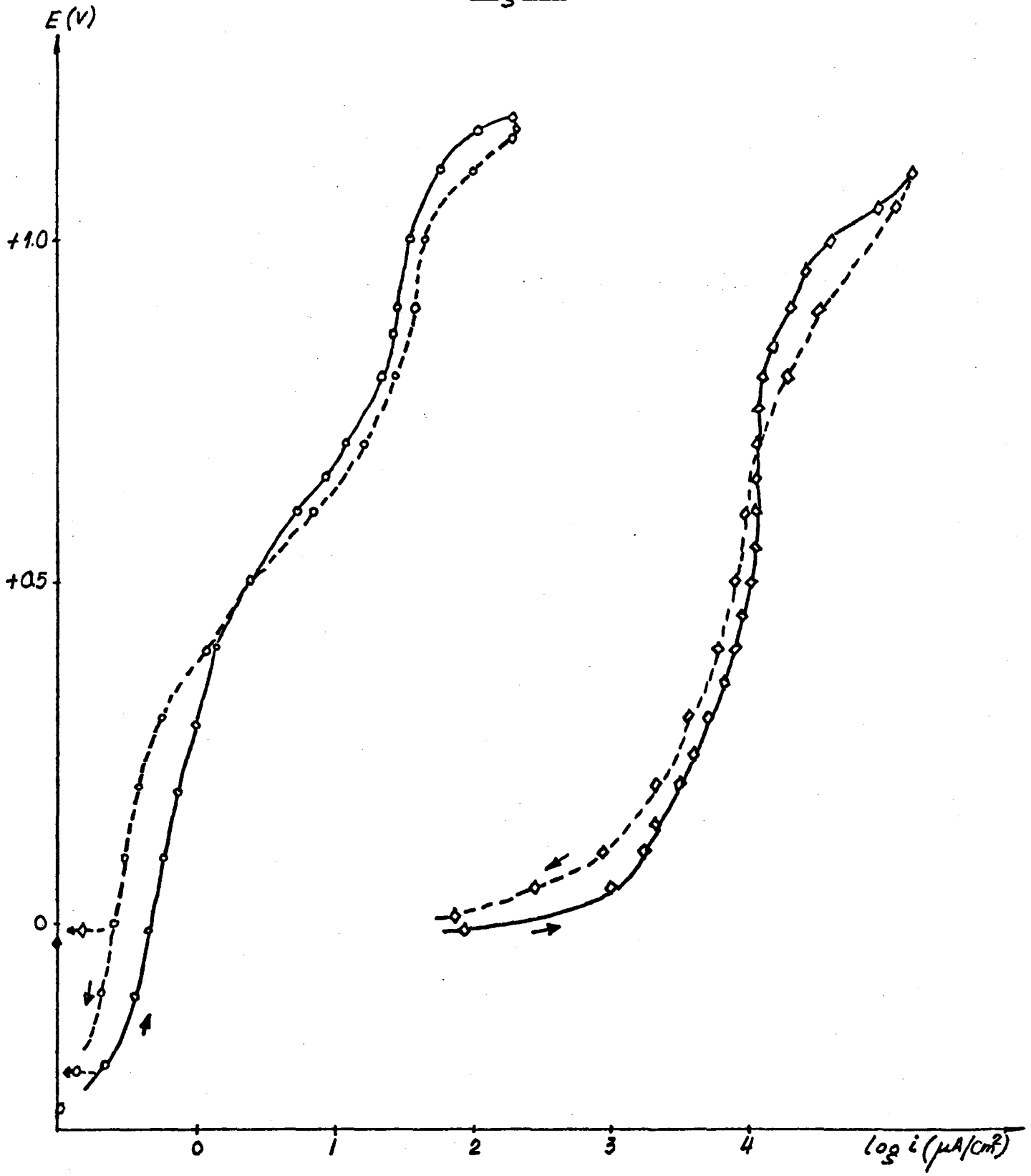

Fig. 20

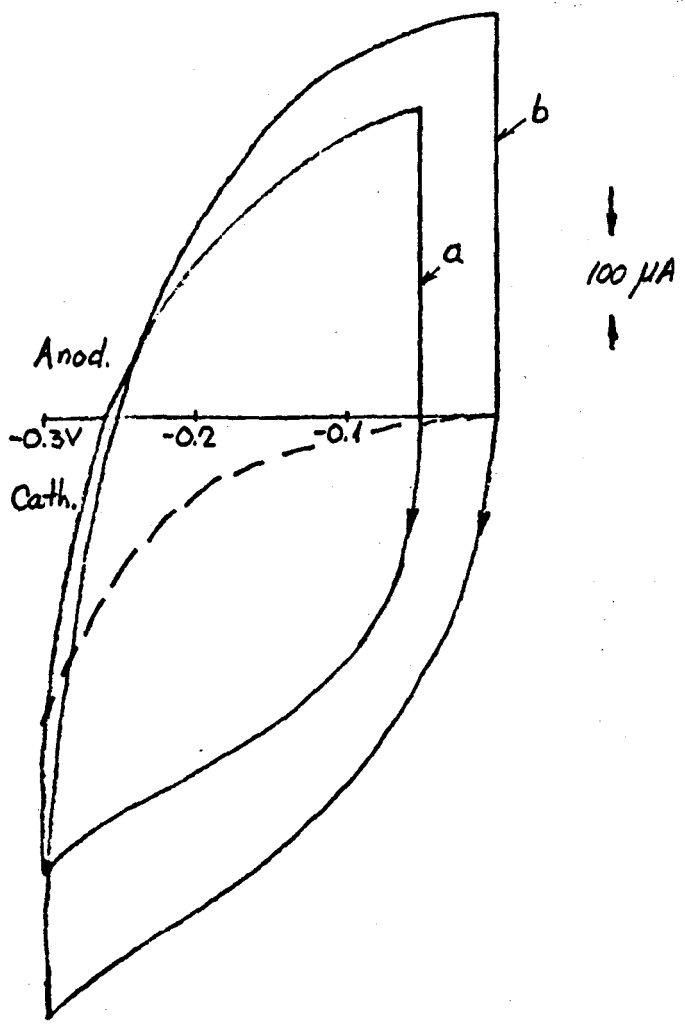

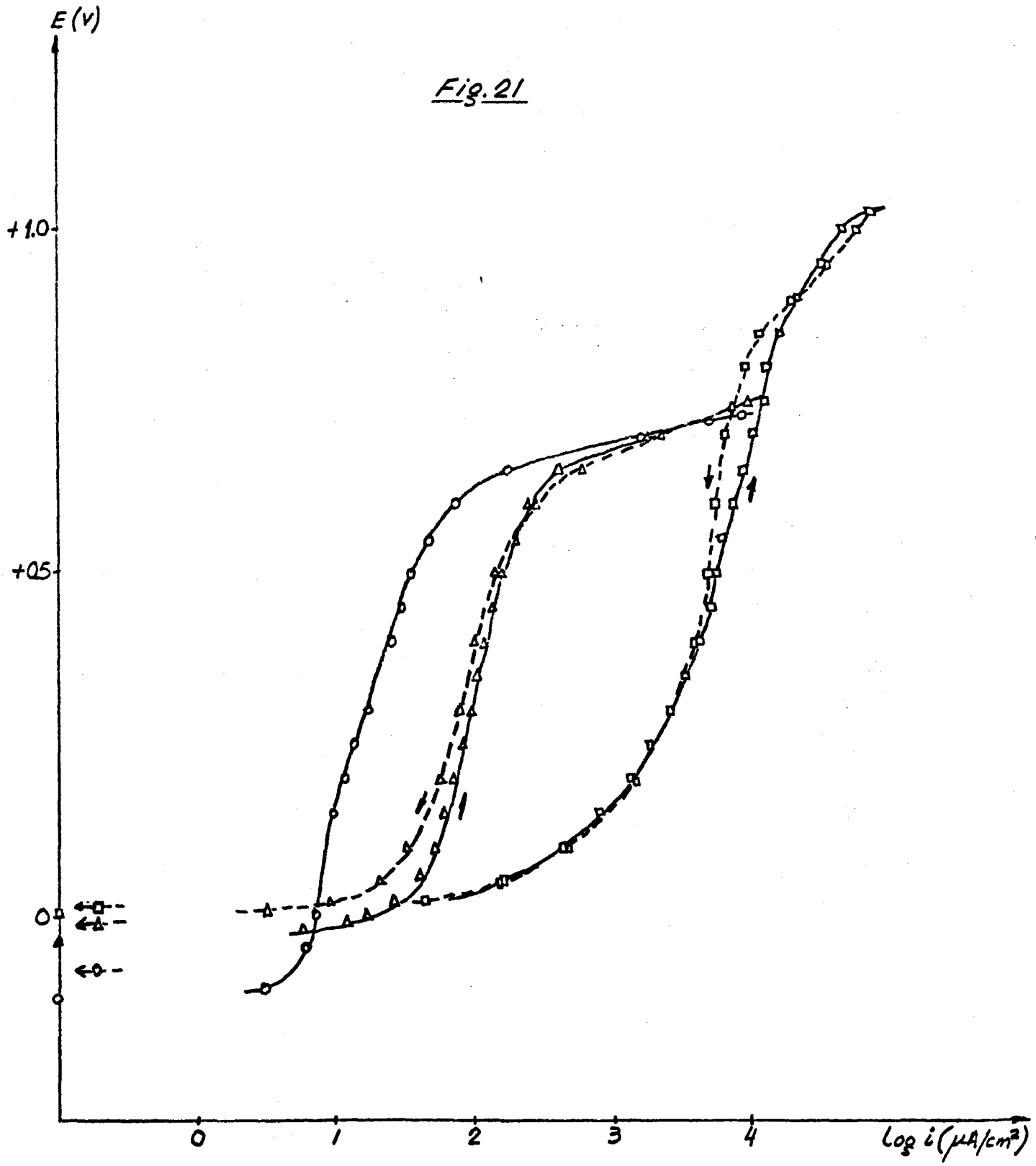

Fig. 21

Fig. 22

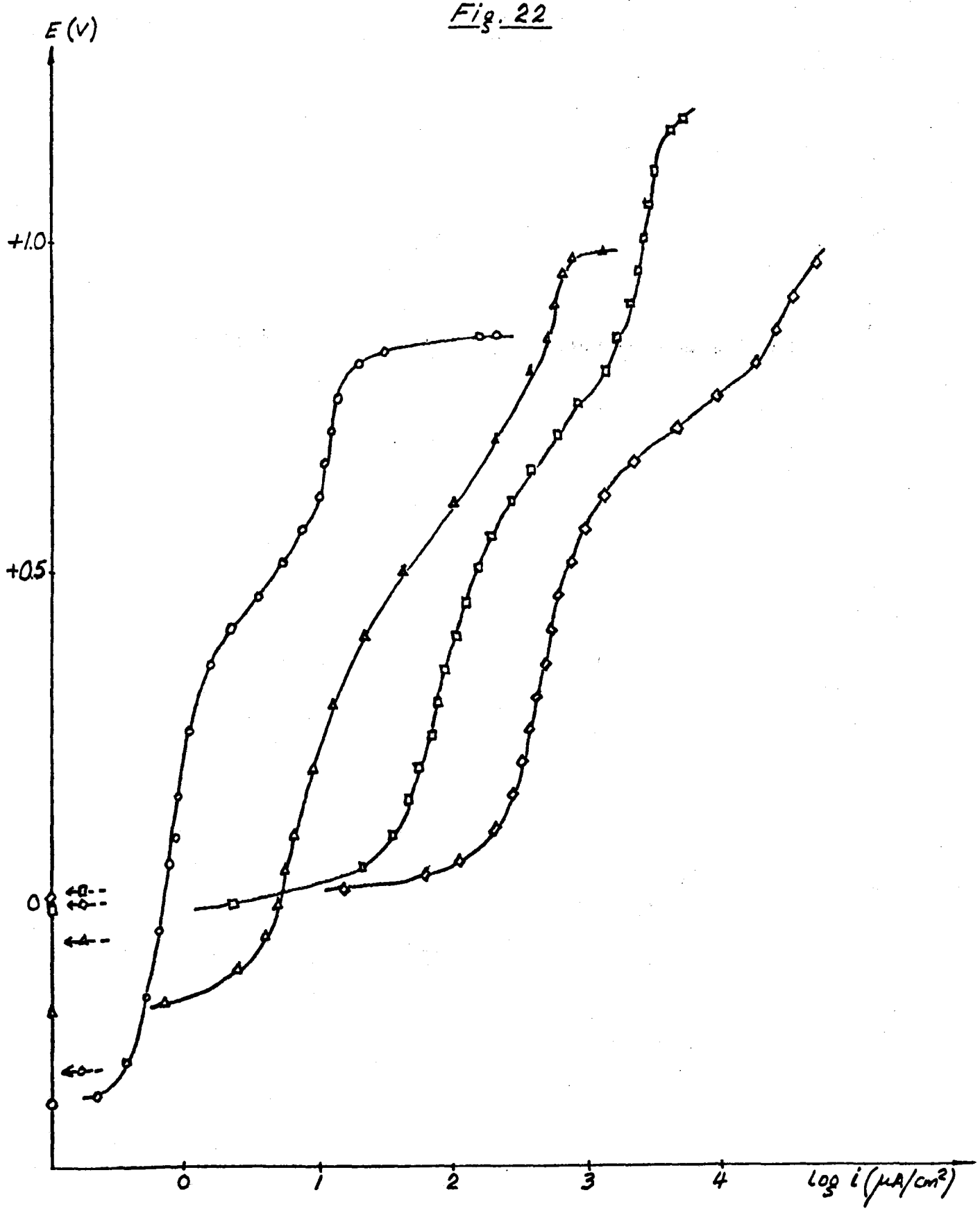

Fig. 23

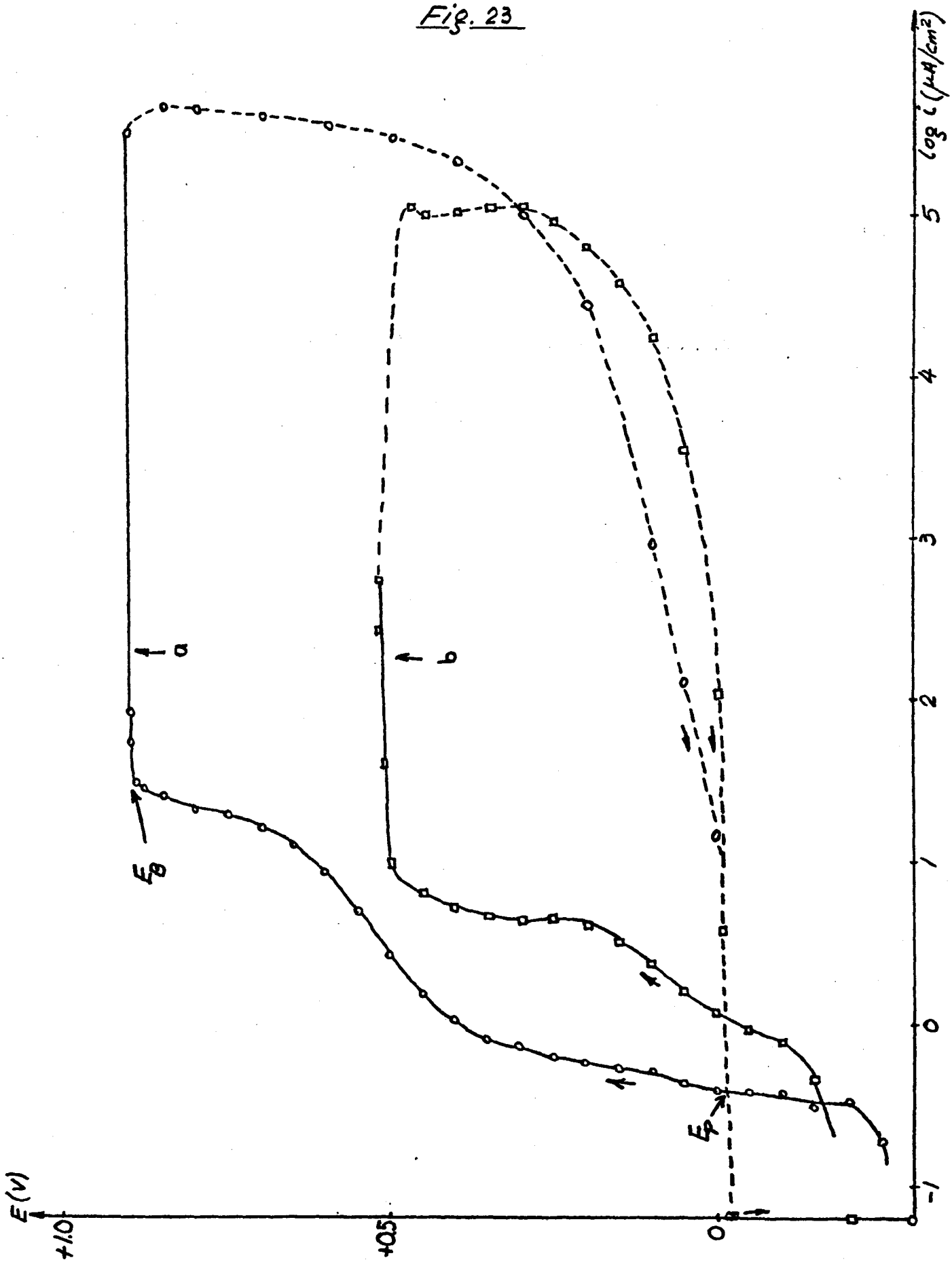

Fig. 24

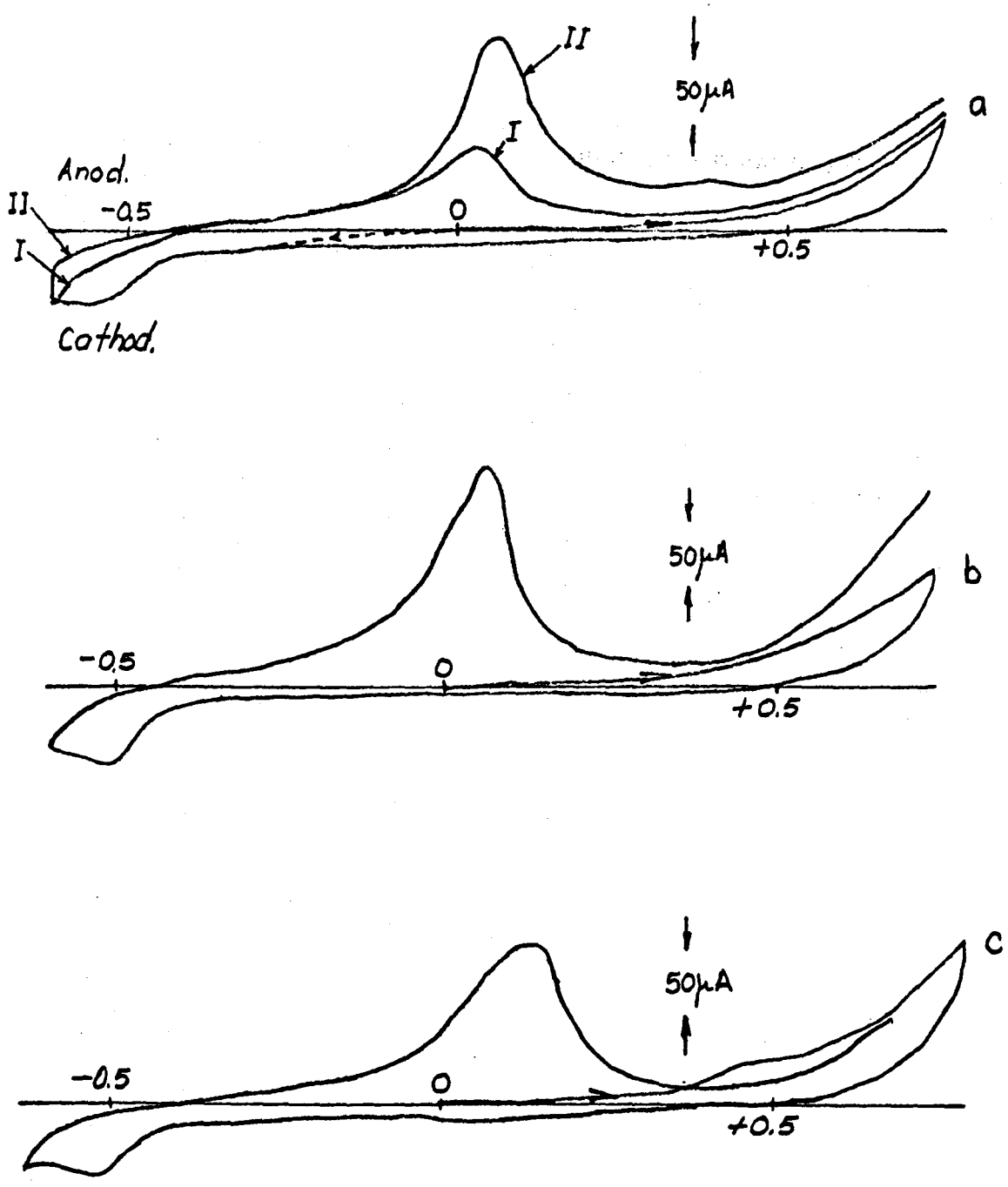

Fig. 25

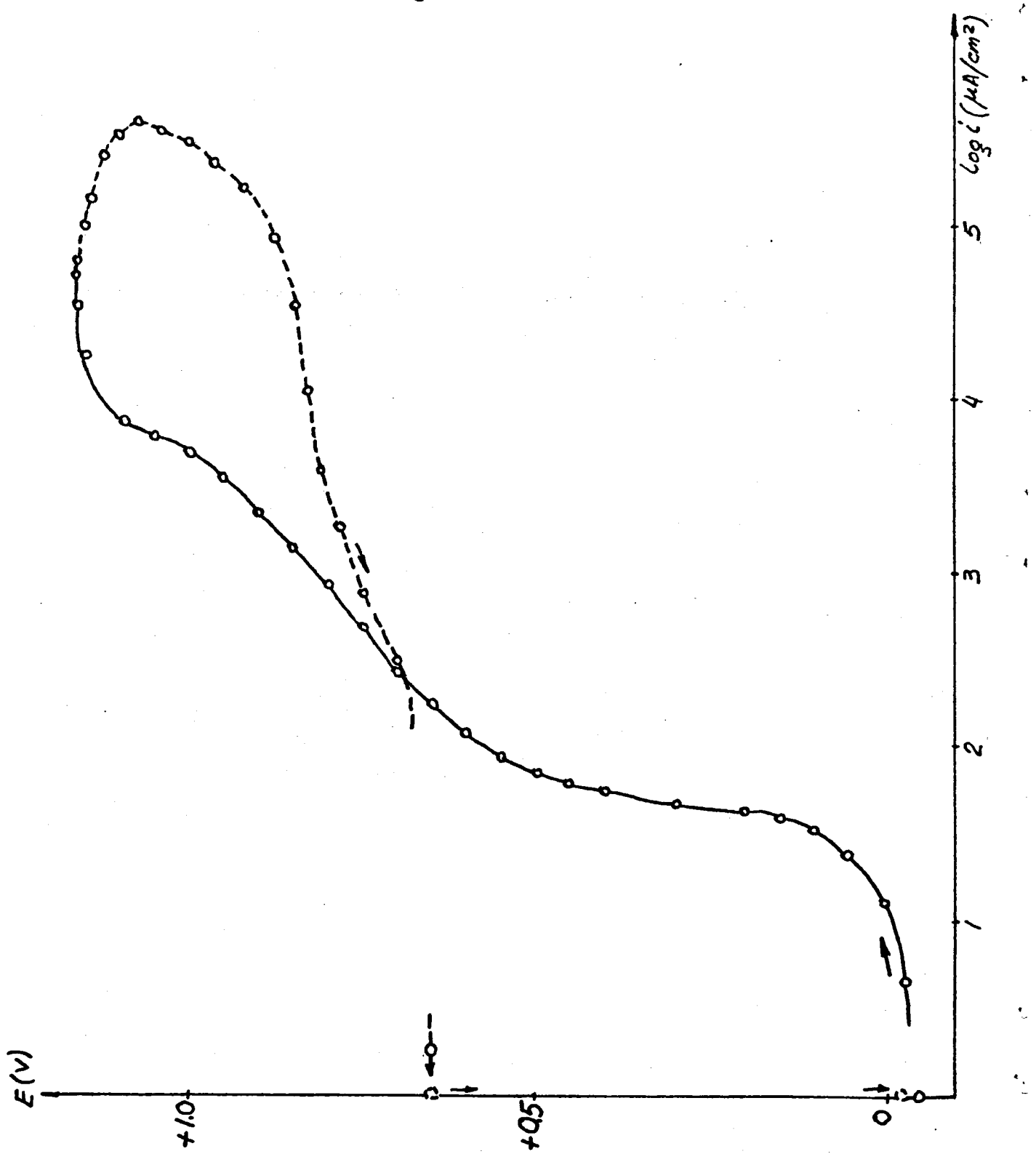

Fig. 26

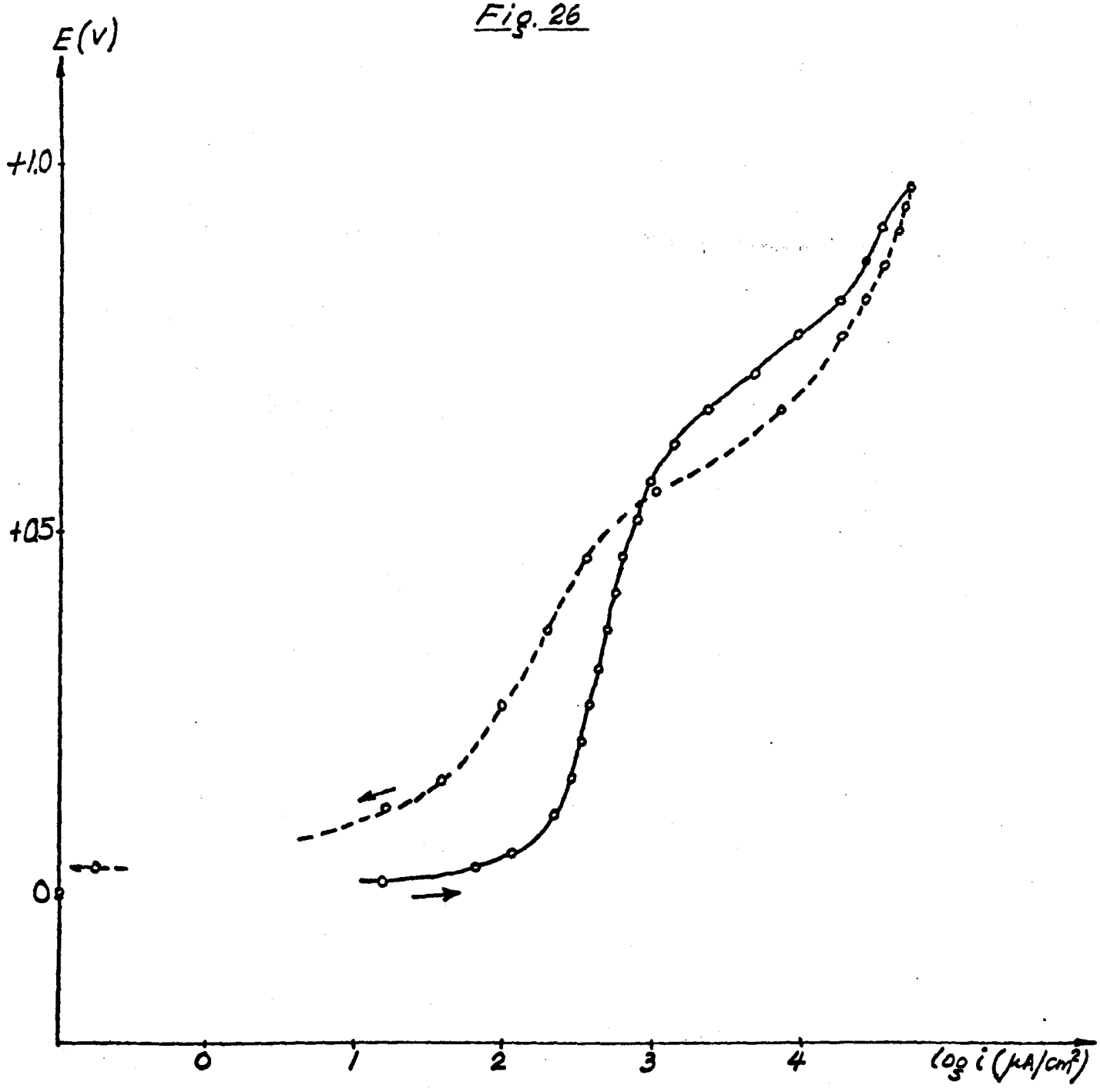

Fig. 27

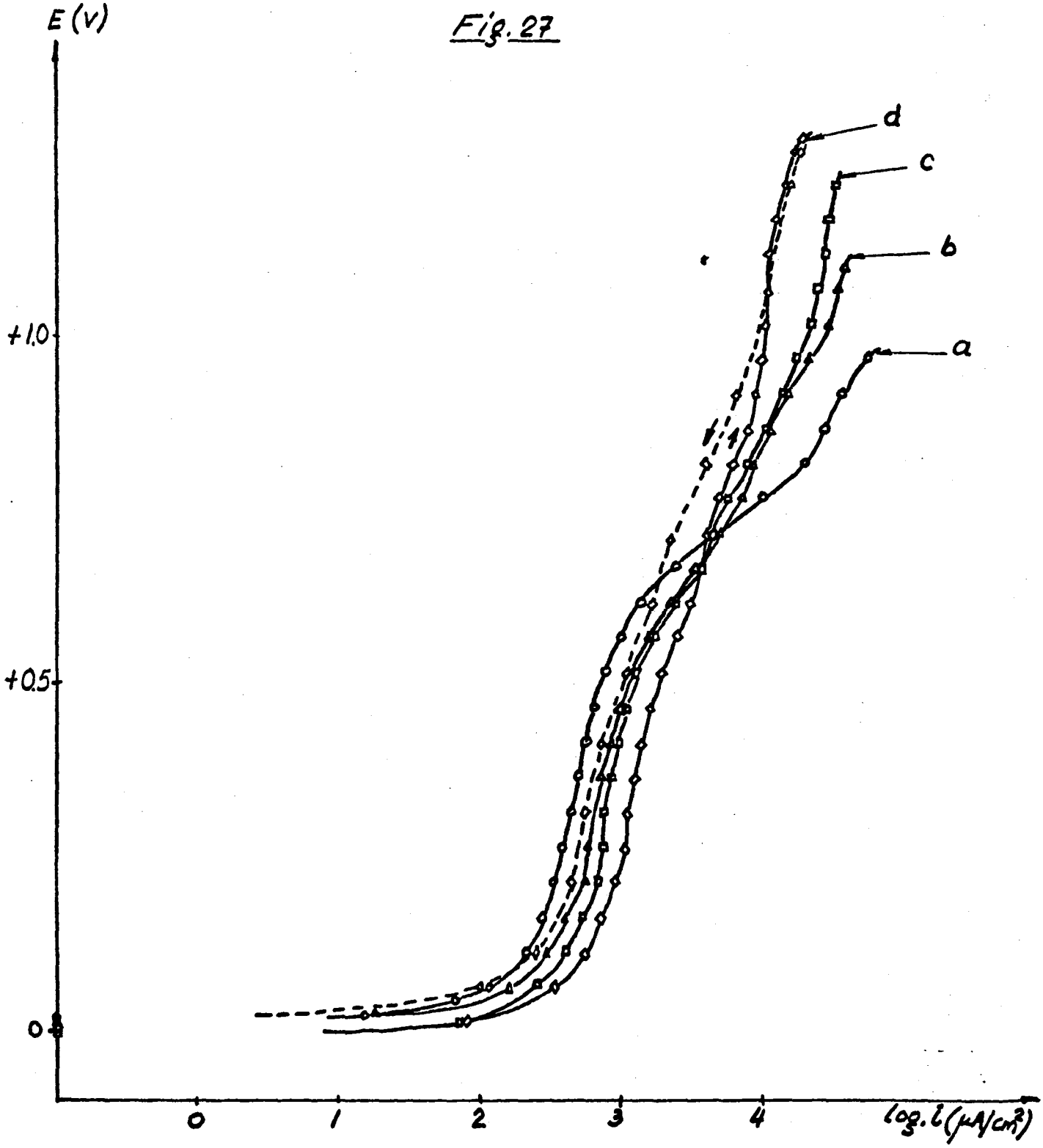

UNLIMITED RELEASE

INITIAL DISTRIBUTION

U. S. Department of Energy (4)
Division of Solar Thermal Technology
James Forrestal Building
1000 Independence Avenue S.W.
Washington, DC 20585
Attn: G. W. Braun
K. T. Cherian
C. B. McFarland
J. E. Rannels

U. S. Department of Energy
Division of Thermal and Chemical Energy Storage Systems
James Forrestal Building
1000 Independence Avenue, S.W.
Washington, DC 20585
Attn: J. H. Swisher

U. S. Department of Energy (2)
San Francisco Operations Office
Division of Solar Technology
1333 Broadway
Oakland, CA 94612
Attn: S. D. Elliott
R. W. Hughey

Aerospace Corporation
P. O. Box 92957
Los Angeles, CA 90009
Attn: P. Mathur

Alon Processing, Inc.
Tarentum, PA 15084
Attn: M. Weinbaum

Arizona Public Service Co.
P. O. Box 21666
Phoenix, AZ 85036
Attn: E. Weber

Babcock & Wilcox
20 S. Van Buren Avenue
Barberton, OH 44203
Attn: G. Grant

Badger Energy, Inc.
One Broadway
Cambridge, MA 02142
Attn: C. A. Bolthrunis

Bechtel Corporation (2)
P. O. Box 3965
San Francisco, CA 94119
Attn: E. Lam
R. Lessley

Black & Veatch Consulting Engineers (2)
P. O. Box 8405
Kansas City, MO 64114
Attn: J. E. Harder
J. C. Grosskreutz

Combustion Engineering, Inc.
1000 Prospect Hill Road
Windsor, Connecticut 06095
Attn: G. H. Rowe

Electric Power Research Institute
P. O. Box 10412
3412 Hillview Avenue
Palo Alto, CA 94303
Attn: J. Bigger

Energy Concepts Co.
627 Ridgely
Annapolis, MD 21401
Attn: D. C. Ericksen

Foster Wheeler Development Corporation
12 Peach Tree Hill Road
Livingston, NJ 07039
Attn: R. J. Zoschak

Gas Cooled Reactor Association
3344 N. Torrey Pines Road
La Jolla, CA 92137
Attn: D. J. Spellman

General Atomic Company (2)
P. O. Box 81608
San Diego, CA 92138
Attn: T. H. VanHagen
J. L. Kaae

Public Service Company of New Mexico
P. O. Box 2267
Albuquerque, NM 87103
Attn: D. J. Groves

Rockwell International
Energy Systems Group
8900 De Soto Avenue
Canoga Park, CA 91304
Attn: T. H. Springer

Sierra Pacific Power Company
P. O. Box 10100
Reno, NV 89501
Attn: R. G. Richards

Solar Energy Research Institute (5)
1617 Cole Boulevard
Golden, CO 80401
Attn: B. Butler
T. Coyle
B. P. Gupta
B. P. Lefferdo
SERI Library

Southern California Edison (2)
P. O. Box 800
Rosemead, CA 91770
Attn: J. N. Reeves
R. S. Williamson

Southwestern Public Service Company
P. O. Box 1261
Amarillo, TX 79170
Attn: K. Ladd

Solar Thermal Systems
Division of Exxon Enterprises, Inc.
P. O. Box 592
Florham, NJ 07932
Attn: P. Joy

Stearns-Roger Engineering Corporation
P. O. Box 58888
Denver, CO 80217
Attn: W. R. Lang

Jet Propulsion Laboratory (2)
4800 Oak Grove Drive
Pasadena, CA 91103
Attn: J. Becker
V. Truscello

Martin Marietta Corporation (2)
P. O. Box 179
Denver, CO 80201
Attn: T. R. Tracey
R. K. McMordie

McDonnell Douglas Astronautics Company (5)
5301 Bolsa Avenue
Huntington Beach, CA 92647
Attn: R. Easten
D. L. Endicott
L. Dreier
C. M. Finch
R. Riedesal

Oak Ridge National Laboratory
P. O. Box X
Oak Ridge, TN 37830
Attn: J. H. DeVan

Olin Corporation (2)
275 Winchester Avenue
New Haven, CT 06511
Attn: L. C. Fiorucci
S. L. Goldstein

Olin Corporation (2)
120 Long Ridge Road
Stamford, CT 06904
Attn: N. Christopher
R. E. Smith

Dr. Robert A. Osteryoung
Department of Chemistry
State University of New York at Buffalo
Buffalo, NY 14214

Pacific Gas and Electric Company (2)
Department of Engineering Research
3400 Crow Canyon Road
San Ramon, CA 94583
Attn: H. E. Seielstad
J. Raggio

Park Chemical Company
8074 Military Avenue
Detroit, MI 48204
Attn: R. W. Foreman

United Engineers and Construction
30 S. 17th Street
Philadelphia, PA 19103
Attn: A. Rosica

General Electric Company
3172 Porter Drive
Palo Alto, CA 94304
Attn: F. F. Witt

West Texas Utilities Company
P. O. Box 841
Abilene, TX 79604
Attn: R. R. Stanaland

J. K. Galt, 1000
M. J. Davis, 1830
R. W. Rohde, 1832
N. J. Magnani, 1840, Attn: R. B. Diegle, 1841
E. H. Beckner, 9700
D. G. Schueler, 9720
R. S. Claassen, 8000, Attn: D. M. Olson, 8100
A. N. Blackwell, 8200
D. L. Hartley, 8500
L. D. Bertholf, 8120, Attn: R. J. Gallagher, 8124
B. F. Murphey, 8300
D. M. Schuster, 8310
D. A. Nissen, 8312
R. W. Mar, 8313
R. W. Bradshaw, 8313
R. W. Carling, 8313
A. S. Nagelberg, 8313
J. C. Swearengen, 8316
S. H. Goods, 8316
L. Gutierrez, 8400
R. C. Wayne, 8430
J. B. Wright, 8450
A. C. Skinrood, 8452
W. G. Wilson, 8453
D. B. Dawson, 8453 (10)
Publications Division, 8265, for TIC (2)
Publications Division, 8265/Technical Library Processes Division 3141
Technical Library Processes Division, 3141 (3)
M. A. Pound, 8214, for Central Technical Files (3)